**Ph.D. Dissertation of Engineering**

# Effect of Al site on dimethyl ether carbonylation reaction in ferrierite zeolite: A First-principles study

# 페리어라이트 제올라이트에서 알루미늄 위치가 디메틸에테르 카르보닐화 반응에 미치는 영향에 대한 제일원리 연구

**August 2021**

**Graduate School of Chemical and biological engineering**
**Seoul National University**

**Hyo Seok Kim**

# Effect of Al site on dimethyl ether carbonylation reaction in ferrierite zeolite: A First-principles study

# 페리어라이트 제올라이트에서 알루미늄 위치가 디메틸에테르 카르보닐화 반응에 미치는 영향에 대한 제일원리 연구

지도 교수 이 원 보

이 논문을 공학박사 학위논문으로 제출함
2021 년 6 월

서울대학교 대학원
화학생물공학부
김 효 석

김효석의 공학박사 학위논문을 인준함
2021 년 6 월

위 원 장 김 도 희
부위원장 이 원 보
위 원 이 규 태
위 원 강 종 헌
위 원 박 명 준

# Abstract

Computational catalysis is one of most fastest growing fields, fueled with the advance in machine learning method and rapid enhancement of computational power, thereby the automation of high throughput screening is achieved. However, this growth is limited by the human understanding level of the catalysis. Especially, Fundamental understanding for heterogeneous catalysis is still not enough to introduce such automation.

In current dissertation, the contents consist of 4 parts. In Chapter 1, my motivation for the research is suggested. In Chapter 2, theoretical backgrounds were covered. The summary of density functional theory and theories for calculating catalytic properties are described.

In Chapter 3, atomistic simulations for heterogenous catalysis model of dimethyl ether carbonylation reaction in ferrierite zeolite. Especially, the role of Al dopant in zeolite and configurations of adsorbate molecular were focused because zeolites are assemblies of some ring units, which results in the structural complexity and ability to molecular sieves.

In Chapter 4, The reaction mechanism of dimethyl ether carbonylation on the active site is suggested and the validation of results is discussed. The whole reaction energies were calculated and the rate determining step was identified. Not only the main reaction paths, but also some side reaction paths were also considered. The results were compared with the literature and discussed.

**Keywords:** First-principles calculation, zeolite, heterogeneous catalysis, dimethyl ether, reaction mechanism, carbonylation

**Student Number:** 2015-22829

# Table of Contents

*Knowledge is one. Its division into subjects is a concession to human weakness.*

*— Halford J. Mackinder*

# List of Tables

# List of Figures

# Chapter 1
# Introduction

## 1.1. Motivation

Research using computation or simulation has been used as a research tool along with experiments for a very long time, but it tends to be used as an auxiliary means of experimentation in that it does not verify validity of itself. However, since numerous simulations and experimental results have recently been integrated into databases and attempts to design machine learning or deep learning models with the help of the database have recently attracted attention, computational research and simulation research go beyond the mere tools of experiments and completely replace the real experiments in a certain area. The paradigm changes in the process.

In the context, rising trend to find out a new catalysis using the automated high-throughput screening using computational material science aggressively occurs. Numerous studies and data have already been accumulated in the field of catalysts, but at the same time, there are many factors that affect catalyst performance. Therefore, it is very difficult to accurately design a new catalyst with desired properties because desired data cannot be obtained in all dimensions no matter how much data is available.

Nevertheless, the scaling relation study can be used as a tool to explain the statistical correlation between certain factors and catalyst performance [1–6]. For

example, it was revealed through the scaling relation that the relationships between the adsorption energy and activation energy of simple molecules such as methane [7–11] and oxygen [12] on metal catalysts are correlated among various metal catalysts. This became a steppingstone for the activation energy value, which is difficult to obtain through experiments or calculations, to be obtained with a simple first-order equation of a simple calculated value such as the adsorption energy. Brönsted-Evans-Polanyi (BEP) relation contributed to the calculation of numerous catalytic reactions [3]. In summary, the scaling relation study is a good approach to understand the change of a multidimensional catalyst performance function for some specific variables, and it was found that there are many linear correlation pairs between catalytic properties such as activation energy and adsorption energy. Thus, the scaling relation make it possible to predict the catalytic properties under a specified condition.

Recently, Machine learning (ML) or deep learning is used to build a prediction model to enhance the previous prediction model. Machine learning model makes it possible to predict the properties of an unknown materials, such as atomization energy [13] , formation energy [14] , density of states [15,16] , band gaps [17,18], and vibrational frequencies [19]. Especially, Artificial neural network enhanced the precision of these models. Crystal graph convolutional neural network (CGCNN) [20] using about 10 thousands DFT calculation data achieved very high prediction accuracy of bandgap, formation energies.

Based on the prediction models, inverse design for discovery new catalyst has been developed. However, there is a large gap between these single-property prediction models and those that predict the performance of a catalyst. This is

because, the interaction of numerous properties must be included to accurately predict the properties of a catalyst. The scaling relation and ML model contributed greatly to predicting specific properties with amazing accuracy or revealing the interrelationship of two different properties, but as mentioned above, catalyst performance is a multidimensional function, so it is very important to accurately grasp the correlation between the prediction and each variable. Moreover, the correlation between variables may not be linear correlated. In this respect, machine learning models for predicting catalyst performance are still in their infancy.

To elucidate the problem of correlation between variables, it is essential to build a universal database, which including the various properties such as material properties of catalysts, reactant and products, and reaction properties. The database such as Materials Project [21], NOMAD [22] and AFLOW [23] gives a great number of calculation data can be partially useful, but not enough called as “universal database” because they only focus on material properties, not lacks catalytic reaction data. One of the universal databases for catalytic properties is catalysis-Hub [24]. It has the information of reaction on catalytic surface, reactants, and product, but their species are smaller than that of other material databases. Thus, universal catalytic database is needed though there exist database for material science.

There are several ways to build a database. One way is to collect data from a published journal papers and build it up in a database. This has advantage of being able to collect many data from people but probably not be able to get all data that I want on the target system and not be able to standardize calculation settings as one database. Because of this, it has recently become common to create various data to

build a database. Fortunately, remarkable advances in the speed and capacity of computer hardware have made it much easier to create databases through computerized automation. This method has the advantage of being able to calculate the desired data on the target system with standardized calculation settings and automatically embed in the database. This makes it possible to build a database much faster and more accurately than in the past when existing data was manually collected, classified, and updated as a database.

Tran et *al.* suggested a promise automated workflow to create a database for discovery of new catalysts based on surface reactions [25]. Here again, the author points out that the database construction for catalytic reaction is still at an infant stage, and a structure should be created that repeatedly cycles through various tasks interlocking like gears, rather than simply constructing a database. The workflow is composed of three categories and the intersection between them. These three categories are database, workflow management, and the surrogate model.

The database is literally a database that contains information on various substances, and it can include all the database such as the Atomic Simulation Environment (ASE) database [26] using custom SQL schema, OQMD [27] using Mongo scheme, and materials project [28], AFLOW [23], NOMAD [22], etc. as mentioned above.

The important thing is to effectively process or organize data types using APIs suitable for each database. It can be called Workflow management that makes this possible. Because workflow management can include a normal research process, if it is well designed, research can be performed much more automatically. In

computational research, it is mainly represented by software that manages the work process of numerous calculations. Finally, the surrogate model builds a predictive model using this database and workflow management. All statistical methods such as scaling relation and ML can be included. This includes developing a descriptor that can show the catalyst performance by deriving a correlation between properties or using physical insight. As all these three tasks are repeatedly performed, when forward feedback to each other occurs, the database becomes more accurate and massive, and it can come closer to a model that can predict catalyst performance.

Consequently, our scientific understanding must be advanced to design new catalysts. Fig. 1 shows the estimated difficulty for automating a type of task versus the field's current scientific understanding. It means that expand of the automation is limited by our fundamental understandings for heterogeneous catalysts. The reason is that even if an incredibly accurate predictive model can be developed, the model is limited by information from the existing database. It cannot change the database itself. However, if our scientific understanding improves, this will be reflected in the database architecture, which will become training data for the development of more accurate models.

Thus, I would like to broaden the understanding of fundamentals for heterogeneous catalysts and contribute to achieve the improvement of automation through the current study. In this dissertation, I would like to focus on the zeolite, which is one of the most wide-used catalysts.

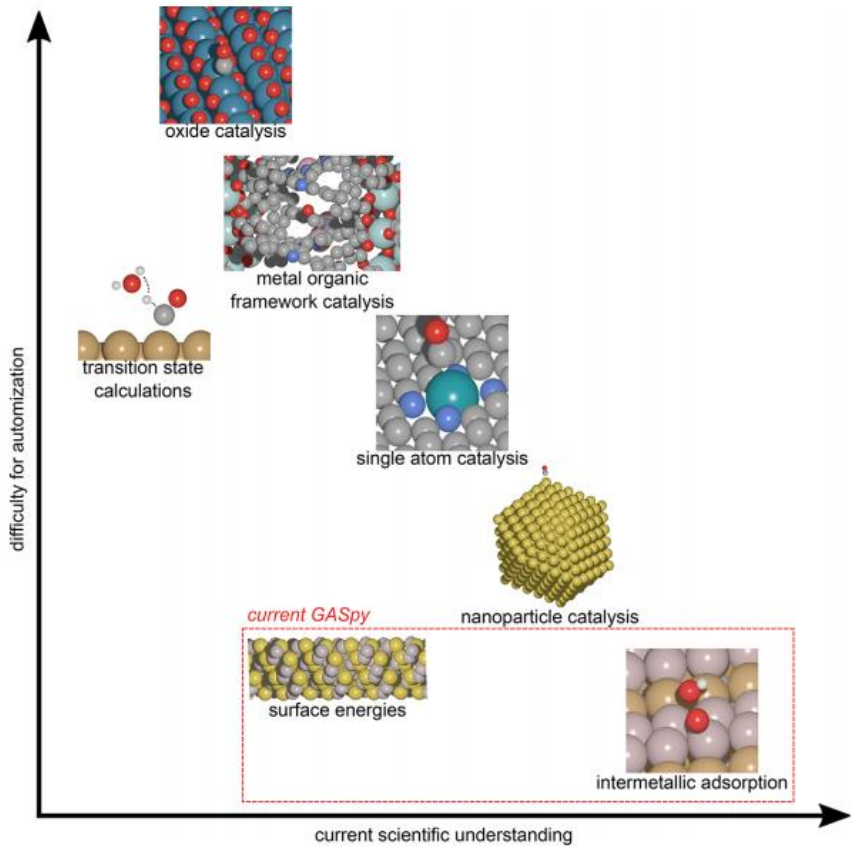


**Fig. 1 Estimated difficulty for automating a type of task vs the field's current scientific understanding. Adapted with permission from [25]. Copyright (2018) American Chemical Society**

## 1.2 Catalytic application of zeolites

In this section I would like to brief the history zeolite research focused on its application as a catalyst for DME synthesis and carbonylation reaction. In addition, I would like to trace the effect of Aluminum distribution on catalytic performance of zeolites.

Zeolites are microporous aluminosilicates, made from corner sharing $SiO_4^-$ and $AlO_4^-$ tetrahedra. Zeolite is composed of cages, pores, channels of various sizes, and its reactivity and selectivity are dependent on the relative size between the components of zeolite and reactant molecules. The structural database of whole zeolites is well established in the International Zeolite Association database [29]. More than 200 unique zeolite frameworks have been identified, while many more theoretical structures are thought to exist [30]. Zeolites are present in our daily life and are used as sorbents, as ion exchangers in detergents or as catalysts in industrial processes as well as in oil refining or petrochemicals as well as in fine chemistry. The uniformity of unique microporous structures also makes them useful as molecular sieves [31].

Among these uses of zeolite, the use as a catalyst has recently received attention due to the green chemistry. Recent concerns regarding global warming and fossil fuel depletion have sparked interest in zeolites as potential catalysts for converting alternative sources, such as shale gas and biomass, to value-added products via C1-3 chemistry [32]. The chemistry of C1 molecules includes carbon monoxide (CO), carbon dioxide ($CO_2$), methane ($CH_4$), methanol ($CH_3OH$), and formic acid (HCOOH). These molecules play an important role in that they are

main precursors in producing high-value chemicals. Since these molecules are usually stable, it is difficult to induce reactions. Nonetheless, if they can be used as an energy source, the environmental benefits that can be obtained are very large, attracting the attention of many researchers.

Various studies have been conducted to convert C1 molecules into other high value-added chemicals. Reactions such as methanol synthesis [33] , dimethyl ether (DME) synthesis [33–35], light olefin synthesis [32,36–38], and methane aromatization [39–41] have been studied in various approaches.

Zeolites have attracted attention due to the potential of an alternative catalyst in C1 chemistry. In the past, metal catalysts such as Rh, Ir, and its organometallic complexes were mainly used for C1 reactions in harsh operating condition because C1 molecule are too stable to react in a normal reaction condition. However, because of the important environmental friendliness of these processes, metals and their complexes are not environmentally friendly, so the need for alternative catalysts has emerged. Since zeolite is very cheap and the composition of the material is eco-friendly, if the existing metal catalyst can be replaced with zeolite, it is possible to guarantee both economic efficiency and eco-friendliness at once.

Attempts to utilize zeolites as catalysts in C1 chemistry have paid off [32,33,42]. Methanol-to-hydrocarbons (MTH) technology has been commercialized to produce gasoline, aromatics, and olefins, including propylene. The gasoline produced through MTH has an advantage in that it has little nitrogen or sulfur impurities such as $SO_x$ or $NO_x$. Thus, the gasoline produced through MTH

can be more eco-friend fuel than gasoline from petroleum. Fe/ZSM-5 based heterogeneous catalysts are used to MTH process [36,43,44].

Another promise process for commercialization is methanol-to-DME reaction [33–35]. DME has attracted an attention as a promise clean fuel. Since DME does not have C-C bond in their molecular structure, its combustion emission products have little amount of unburn molecule such as CO, and hydrocarbons compared to natural gas. For the DME synthesis, hydrophobic zeolites are well-known for their high catalytic selectivity and reactivity. As zeolite is widely used for the synthesis of olefin, gasoline, and DME, a considerable amount of research on zeolite catalysis has been performed to understand its properties [45–47].

In summary, zeolite is newly attracting attention as the most promising candidate for an eco-friendly catalyst, and research to apply zeolite to various processes and eco-friendly fuel production and conversion have been being conducted. Among them, we will focus on the DME carbonylation reaction, and in the next chapter, we will introduce several examples of how computational chemistry and First-principles calculations can be applied to study this reaction.

## 1.3 Computational modeling of catalytic reaction in zeolite

Using a computational chemistry is a paradigm-shift approach in contrast to the trial-and-error method that has been used for decades [45], as it can rapidly replace conventional experimental tools, including infrared (IR), X-Ray Diffraction (XRD), Raman spectra. First-principles modeling is a combination of solid states physics and surface chemistry [49]. It can be used to find the electronic structure of a catalyst, which relates to its reactivity on the surface, where the bonds of reactant molecules break to form new bonds. Previously, detailed reaction mechanisms

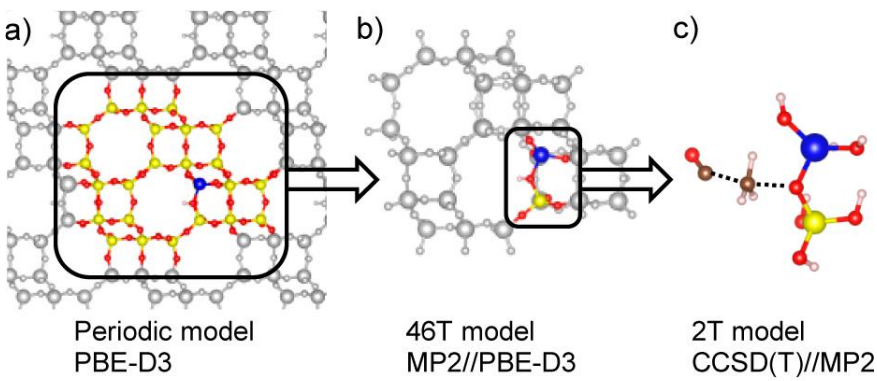


**Fig. 2 Models of the zeolite catalysts.**

**(a) periodic model with DFT Perdew–Burke–Ernzerhof (PBE)-D3 method, (b) 46 atomic cluster model with Møller-Plesset perturbation theory (MP2)/ PBE-D3 method, and (c) 2T cluster model with coupled-cluster method (CCSD)(T)/ MP2 method. Reprinted with permission from [48]. Copyright (2017) American Chemical Society.**

were hard to completely understand because the reaction networks are very complex and little was known about their physicochemical exactness [50]. First-principles approach makes it possible to analyze a specific elementary reaction of a reaction system, thereby shedding light on the reaction mechanisms on many catalytic systems.

One of important point in understanding the catalytic performance of zeolite is the concentration and distribution of Brønsted acid sites in zeolite frameworks. A Brønsted acid site of Al-substitute zeolite is commonly accepted to initiate MeOH adsorption, followed by its dehydrogenation reaction. In 1995, Haase et al. [51] succeeded in calculating the interaction of MeOH with a Brønsted acid site of simple zeolite structure using the second-order Moller-Plesset perturbation theory (MP2) (Fig. 2). Their calculations showed a reasonable match to experimental results. They also observed that the OH stretching frequencies of MeOH changed due to the electronic correlation with the acid site of the catalyst, which is consistent with the IR spectroscopy results.

Recently, Plessow et al. [48] calculated the H-SSZ-13 using a hierarchical cluster approach to secure an acceptable level of accuracy, which could provide a detailed mechanism of MeOH dehydrogenation reaction. They performed quantum chemical calculations at different levels in different models to ensure the accuracy of their results. Their work is the first reported to accurately calculate the transition states and activation energy of the MeOH dehydrogenation reaction, which is significant not only for MeOH to DME, but also for MeOH to olefins reactions.

The conversion of dimethyl ether (DME) to methyl acetate (MA) in the 8-membered ring (8MR) is considered as an example to show the dependence of catalytic reactivity on the position and distribution of Al in the zeolite. Cheung *et al.* reported that H-mordenite (H-MOR) and H-ferrierite (H-FER) zeolite catalyzed the conversion of DME to MA with a stable reaction rate and >99% selectivity at low temperatures (423–463 K) [52]. The reaction mechanism was suggested as follows:

$$R_1: \text{Z-H} + \text{DME} \rightarrow \text{Z-CH}_3 + \text{H}_2\text{O} \quad (2)$$

$$R_2: \text{Z-CH}_3 + \text{CO} \rightarrow \text{Z-CH}_3\text{CO} \quad (3)$$

$$R_3: \text{Z-CH}_3\text{CO} + \text{DME} \rightarrow \text{Z-CH}_3 + \text{MA} \quad (4)$$

The methyl group produced by the dissociation of DME ($R_1$) combines with CO to form an acetyl group ($R_2$), which reacts with DME to produce MA ($R_3$). The rate-determining step (RDS) of the mechanism was verified to be $R_2$ by kinetic experiments and nuclear magnetic resonance (NMR) spectroscopy [53]. Bhan *et al.* found that the carbonylation reaction only occurred in the zeolites, which consist of the 8MR site [54]. The number of BAS within 8MR channels was measured by the rigorous deconvolution of the infrared bands for BAS in H-MOR and H-FER, and the MA production rate was proportional to the number of BAS within 8MR.

Boronat *et al.* explained the attribute of the BAS in the 8MR cage of the zeolite using first-principles calculations on H-MOR [55]. The activation energies of the methyl group by four attacking molecules (CO, $CH_3OH$, DME, and $H_2O$) were calculated at each T-site in H-MOR, as follows:

$R_4$: $Z\text{-}CH_3 + CO \rightarrow Z^- + CH_3CO^+$ (5)

$R_5$: $Z\text{-}CH_3 + CH_3OH \rightarrow Z^- + (CH_3)_2OH^+$ (6)

$R_6$: $Z\text{-}CH_3 + DME \rightarrow Z^- + (CH_3)_3O^+$ (7)

$R_7$: $Z\text{-}CH_3 + H_2O \rightarrow Z^- + CH_3OH_2^+$ (8)

It was shown that DME could access the methyl group on the T sites to produce trimethyloxonium ($R_6$), except for the T3-O33 position, where the activation energy for $R_6$ is higher than that of $R_4$ due to the steric hindrance of DME resulting from the unusual orientation of the methyl group at T3-O33 in the 8MR, indicating that the unique selectivity appears only at the T3-O33 position.

The Al distribution can significantly influence the BAS in 8MR and the reactivity of the DME carbonylation reaction. Li *et al.* have quantitatively verified that the formation rate of MA by DME carbonylation reaction is proportional to the concentration of BAS in 8MR [56], which could be controlled by introducing of various organic structure-directing agents (OSDAs) for the synthesis of the H-MOR structure. It was also shown that the strength of the interaction between the amine or sodium cation and $[AlO_4]^-$ played an important role in the Al distribution. The stronger the interaction, the higher the number of Al in the 8MR, and the corresponding BAS concentration.

Jung *et al*. found that ferrierite zeolite synthesized by the seed-derived hydrothermal method without any OSDA had a high catalytic reactivity for DME carbonylation to MA [57] because recrystallization during the preparation step resulted in high crystallinity for many BAS in 8MR. In the subsequent study, the

most active aluminum location that drastically enhanced the carbonylation rate was identified and the strength of the degree of the interaction between BAS and DME was calculated by first-principles calculations [57]

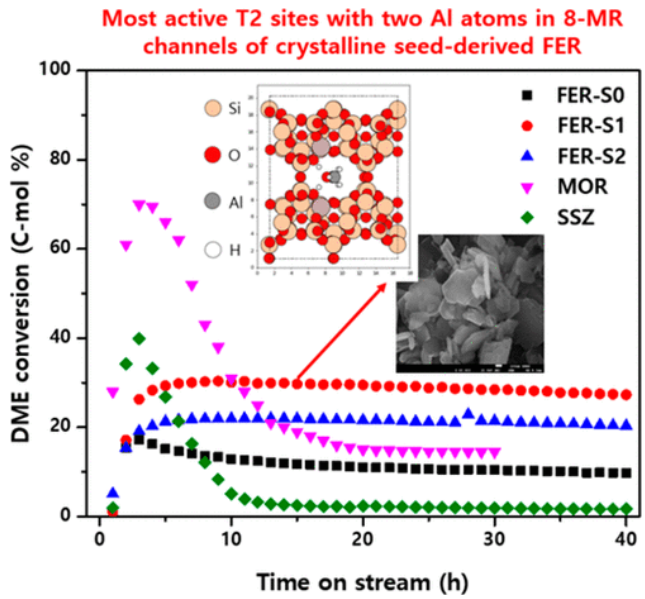


**Fig. 3 DME conversion over seed-derived ferrierite zeolite. Inset pictures show the atomistic location of aluminum for the most active site in 8MR (upper) and the FESEM image of FER-S1 sample (lower). Reprinted with permission from [57] Copyright (2020) American Chemical Society.**

# Chapter 2

# Theoretical backgrounds

Theoretical backgrounds for atomistic modeling methods mainly depend on quantum mechanics and statistical mechanics. In this chapter, basic concepts for the density functional theory (DFT) are introduced. And next, computational methods for thermodynamic properties are described.

## 2.1 Electronic structure calculations

### 2. 1. 1. Schrödinger equation

Modeling the electronic structures aims to get a solution of states of a quantum mechanics system. one of the most important state equations for describing quantum mechanical system is the Schrodinger equation:

$$\widehat{\boldsymbol{H}}\psi = E\psi$$

where, **H** is the Hamiltonian operator, $E$ is total energy of the system, and $\psi$ is a wavefunction which contains all information of the system such as ground-state energy and electron densities. The problem is that the equation only has the analytic solution for the hydrogen atom, other systems cannot be solved analytically. For the N-atoms system, the problem becomes a 3N-dimensional many-body problem. To lower the complexity, many approximations were introduced historcally, and there exist many solutions of these simplified problems of getting electronic structures.

### 2.1.2 Hartree-Fock Method

Hartree-Fock method is one of the simplest approaches to solve the complexity of Schrödinger equation. The solution of the equation can be expressed as a Salter determinant of the one-electron wavefunctions $\psi_i$, which are the eigenfunction of the one-electron Fock operator ($f_i$),

$$f_i\psi_i = E_i\psi_i$$

$$f_i = \hat{T} + \hat{V} + \hat{V}_{H,i} = -\frac{\hbar^2}{2m}\nabla^2 + \hat{V} + \hat{V}_{H,i}$$

where $\hat{T}$ is the operator for the kinetic energy, $\hat{V}$ is the operator for the potential energy due to electron-nucleus interactions, $\hat{V}_{H,i}$ is the operator for the Hartree-Fock potential arising from the electron-electron electrostatic interactions of the *i*-th electron with all other electrons. $\hbar$ is the reduced Planck's constant, m is the electronic mass, $E_i$ is the energy of the one-electron wavefunction $\psi_i$.

### 2.1.3 Density functional theory

One of outstanding works for alternative method for solving Schrödinger equation is the very Density functional theory (DFT), contributed by Walter Kohn and Sham. DFT is based on the premise that the electronic density is a functional of the ground state energy, which is developed by Hohenberg, Kohn, and Sham in 1960s [58]. The Schrödinger equation is transformed by approximations to Kohn-Sham equation, which is,

$$\left[-\frac{\hbar}{2\mathrm{m}}\nabla^2 + \mathrm{V}(\mathbf{r}) + \mathrm{V_H}(\mathbf{r}) + \mathrm{V_{XC}}(\mathbf{r})\right]\psi_\mathrm{i}(\mathbf{r}) = \epsilon_\mathrm{i}\psi_\mathrm{i}(\mathbf{r})$$

The Hamiltonian of the Kohn-Sham equation is like the one-electron Hamiltonian in the HF methods, except for an additional exchange-correlation operator, $V_{XC,}$ which consider many-body electron interactions. The exact solution of the exchange-correlation does not exist, but various approximation of the exchange-correlations functional successfully described the electronics structure of many materials.

## 2.2 Catalytic properties

This section examines the theory of computational chemistry for the catalytic research field, including the theories and calculation methods for calculating adsorption energy, vibrational frequency, and activation energy, to understand the properties of a catalyst, based on the Density Functional Theory(DFT) [58]. The field of DFT has become a starting point for the full-fledged application of computational chemistry and is currently used in various fields.

### 2.2.1. Surface Modeling

For modeling a catalytic reaction, it is essential to build an adequate surface model. The surface model has been developed in various ways along with its purpose. There are three surface models categorized by Sabbe et al. [59], which are a cluster model, embedded cluster model, and periodic model. The cluster model is a model that focuses on the active site and has the advantage of being able to perform efficient calculations with few resources. However, it is difficult to simulate a complex catalyst surface because it cannot consider long-range interactions, such as electrostatic potential. The embedded cluster model makes up for the cluster

model by introducing a simple model for long-range interactions. In the embedded cluster model, a short-range near the active site is calculated by the quantum mechanical approach, and the others are considered as a kind of perturbation. This approach effectively simulates the catalytic reaction, such as $CO_2$ reduction reactions [60]. The periodic slab model can be calculated for an infinitely regular surface that does not consider edges so that an accurate electronic structure for the crystal structure can be obtained. However, to simulate a surface with irregularities, such as defects or impurities on the surface, a supercell is required, which increases the computational cost.

### 2.2.2. Adsorption Energy

Adsorption energy is an important property used to investigate the catalytic reaction as it quantifies the amount or intensity of adsorption when the reactants in the gaseous phase adsorb onto the catalyst surface. The adsorption energy can be determined by calculating the ground state energies before and after adsorption using the DFT calculation, and the difference between them, as follows:

$$E_{ads} = E_{slab+adsorbate} - (E_{slab} + E_{adsorbate}) \quad (1)$$

Early DFT calculations were only marginally able to predict the adsorption energy. Therefore, Feibelman et al. [61] constructed a model for CO adsorption on a Pt(111) catalyst to find the calculated adsorption energies using several XC functionals based on a generalized gradient approximation (GGA), such as Perdew-Wang 91 (PW91), PBE and RPBE, overestimated experimental values. In the 2000s, Kresse et al. [62] introduced the semilocal functional to accurately calculate the adsorption

energy of CO on Pt(111) to compensate for the underestimated value of the gap between the highest occupied molecular orbital (HOMO) and the lowest unoccupied molecular orbital (LUMO). They also demonstrated that the interaction between metal and the $2\pi^*$ orbital was overestimated in conventional DFT calculations, and suggested many alternative correction methods, including DFT + U, a hybrid functional [63,64]. The adsorption energy of many catalytic reactions has been calculated for various metal catalysts other than Pt, and a high consistency between experimental results and calculations has been accomplished. This method was also successfully applied to strongly correlated materials such as NiO [65] as well as other materials [66].

### 2.2.3. Activation Energy

An important property in a catalytic reaction is the activation energy. Activation energy, which has been estimated experimentally in the form of the Arrhenius equation, can be calculated directly using computational chemistry. As activation energy is defined as the difference in energy between a transition state and the initial state, the geometry of the energy of both states must be obtained by the DFT. The most widely known method for directly obtaining the transition state is the nudged elastic band (NEB) method [67,68], where the minimum energy path (MEP) between the states before and after the reaction on the potential energy surface are explored (Fig. 2). A series of atomic configurations between the initial and final states are used for finding the MEP. These configurations describe the reaction pathway and are connected by spring forces in which the distance between configurations is fixed. Thus, the direction of the net force on a configuration is the

sum of three forces; the spring force connected neighbor configuration, perpendicular force induced by the potential energy surface, and the unprojected forces. Through iteration, each configuration moves to the nearest saddle point, and the MEP is found.

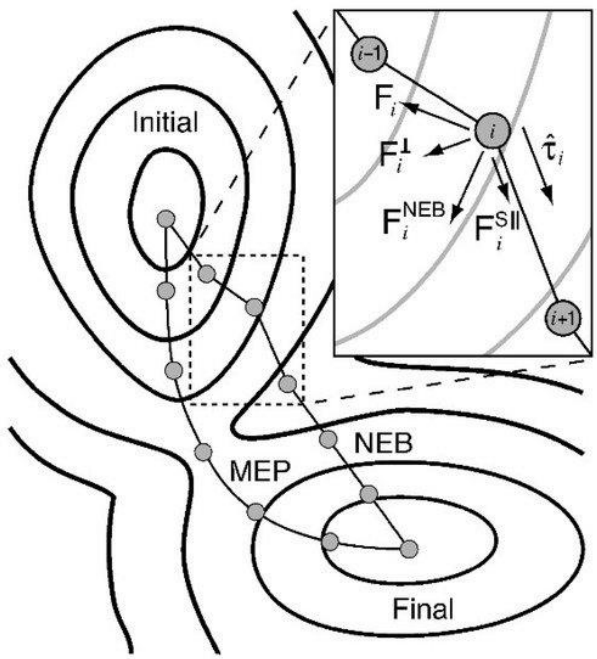


**Fig. 4 Illustration of the nudged elastic band (NEB) method on a potential energy surface (PES)**;

$F_i^{NEB}$: nudged elastic band force, $F_i{}^{S\parallel}$: spring force along the tangential $\tau_i$, $F_i^{\perp}$: perpendicular force, and $F_i$: the other forces. Reprinted with permission from [68]. Copyright (2000) AIP Publishing.

# Chapter 3
# Gas-Phase Carbonylation of Dimethyl Ether on the stable Seed-Derived Ferrierite

## 3.1 Introduction

A gas-phase carbonylation of dimethyl ether (DME) on heterogeneous catalysts is one of the promising alternative pathways to replace a liquid-phase carbonylation using novel metal complexes such as Rh or Ir organometallics [69–71] by selectively producing value-added petrochemicals. The gas phase DME carbonylation to methyl acetate (MA), where DME can be synthesized by $CO_x$ hydrogenation [72–76], has been reported to be active on various acidic zeolites such as a mordenite (MOR) having eight-membered-ring (8-MR) channels where gas-phase DME carbonylation mainly occurs [52,53,77]. The MA formation rate by DME carbonylation has been well reported to be proportional to the number of protonic Brønsted acidic sites in the 8-MR channels, especially on an MOR containing the perpendicularly intersecting 8-MR and 12-membered ring (12-MR) in comparison to other zeolites.[55] In addition, the MA intermediate can be further transformed to various value-added chemicals such as acetic acid and ethanol through hydrolysis or hydrogenation.

However, the highly active MOR generally showed a faster deactivation rate from the very beginning of the reaction due to the preferential depositions of coke precursors in the larger 12-MR channels [78,79]. Therefore, the novel ZSM-35 having 10-MR straight channels perpendicularly located with 8-MR channels instead of 12-MR channels of the MOR was suggested to suppress heavy and aromatic coke precursors by enhancing the diffusion rate of reactants and products in the smaller 8-MR channels. Based on previous works [79,80], the relatively planar FER micropore channels with their perpendicularly intersecting structures of 8-MR and 10-MR channels bridged by 6-MR pockets with fewer defect sites were effective for a superior catalytic stability in comparison to the MOR zeolite. However, the effects of the crystallinity of the FER with its characteristics of surface coke formation as well as Al distributions in the 8-MR channels on the catalytic activity and stability have not been well investigated until now as far as we know, since the FER generally showed a much lower initial activity of DME carbonylation due to the smaller pore structures in comparison to that of the MOR zeolite, which seems to be less effective for the diffusion of reactants and products.

Here, we conducted three types of work. First, the Al distribution in FER zeolite was explored using DFT calculation. All possible configurations in 6-, 8-MR channel were investigated and energies at the configurations were compared. The most stable Al site was identified and verified with experimental data. In addition, the adsorption energy of DME at the configuration was also calculated and the most stable conformation of DME adsorption was identified, which was also compared with experimental data. Finally, we analyzed the results using simple

statistical data process and the limitation of atomistic model and difference between theory and experiments are dealt with.

## 3.2 Calculation details

All density functional theory (DFT) calculations were performed by the projector augmented wave (PAW) formalism, as implemented in the Vienna Ab–initio Simulation Package (VASP) [81,82] The exchange–correlation functional, given by the generalized gradient approximation (GGA) suggested by Perdew, Burke, and Ernzerhof (PBE) [83] was used. The ferrierite unit cell containing 216 atoms ($Si_{72-x}Al_xO_{144}$) was imported from the Materials Project [21]. The structure of FER is depicted in Fig. 11. The T2 and T4 sites each are symmetrically equal at pure FER, but the symmetry is broken when Al atoms were introduced. Therefore, naming four T2 sites as a-d was introduced to distinguish each of the site.

All structures were fully relaxed to a maximum force convergence criterion of 0.01 eV $Å^{-1}$. The energy convergence threshold was set to $1 \times 10^{-8}$ eV. The cutoff energy was set to 400 eV for all calculations. Dispersion correction for the van der Waal interaction was considered by adding a pairwise interaction term to the Kohn-Sham energy using the DFT-D3 approach proposed by Grimme[84] and extended by Kerber et al. [85] which is widely applied for the theoretical investigation of adsorption and reaction in Zeolite. [86]

All adsorption energies were defined by,

$$E_{ads} = E_{FER+DME} - (E_{FER} + E_{DME})$$

where $E_{FER+DME}$, $E_{DME}$, and $E_{FER}$ are the total energies for the adsorption complex, isolated dimethyl ether (DME) molecule, and isolated zeolite, respectively.

## 3.3 Result and Discussion

### 3.3.1 distribution and DME adsorption energy

To verify the stability and strengths of adsorbed DME molecules and Al configurations and locations in the 8-MR channel bridged 6-MR pockets of the FERs, density functional theory (DFT) calculations were performed. The number of Al atoms substituted in the 6-MR pockets of the FER zeolite was varied from one to four Al atoms, and total energies of all the plausible configurations of Al atoms were calculated to find out the most stable structures of the Al atoms in the 6-MR pockets. The typical unit cell configurations of the FER frameworks are displayed in Fig. 11, and all T sites in the 8-MR and 10-MR channels as well as the T2 and T4 sites in the 6-MR channels connected to the 8-MR channels are separately displayed. The most stable structures according to the adjacent number of Al atoms were depicted, and the results are displayed in Fig. 5, where the total energies for all cases are also included in Figs 12−17. Finally, the Brønsted acid sites with different Al configurations and the numbers of Al atoms were estimated, since the Brønsted acid sites in the FER structures can be transferred between the oxygen sites under a higher content of Al species in the FER structures. Based on the present DFT calculations, the FER zeolite having two acidic Al sites in the T2 site which connected the 8-MR channels and 6-MR pockets with 10-MR channels were found to be more stable than other numbers of Al atoms. The most stable

configurations of two Al atoms in the FER structures were found to be the acidic T2 sites with their far opposite locations in comparison to other numbers of Al atoms. This result can possibly be attributed to two factors such as the repulsions between the acidic Al sites in the 6-MR pockets and interactions of the acidic Al sites with adjacent oxygen atoms, which further make it possible to maximize the acidic strengths with two Al sites with their maximum distance. With the calculated stable configurations of Al atoms, the adsorption energy of DME molecules on those acidic Al sites was further calculated and the adsorbed complexes and relative adsorption energies were found to be −0.078, −0.45, −0.0067, and +0.86 eV in terms of the number of Al atoms from one to four (Fig. 5). Similarly, the energies of DME adsorption at different positions of Al atoms in the 8-MR channels were calculated, and the results are summarized in Fig. 10-12 and Table. 1-2. Stable and stronger DME adsorptions were observed on the adjacent two Al atom substituted T2 sites in the 8-MR channels with its lowest energy of −1.691 eV in comparison to those of one and three Al atoms with their separate values of −1.171 and −1.637 eV, respectively, where the DME molecules were preferentially and stably adsorbed on the two closely located Al atoms. The DFT calculation results strongly suggested that the adsorption energy of DME molecules on two adjacent Al atoms in the 6-MR pockets and 8-MR channels with the next-next-nearest Al−O−Si−O−Si−O−Al configurations can be minimized to form more strongly adsorbed intermediates on the Brønsted acid sites.

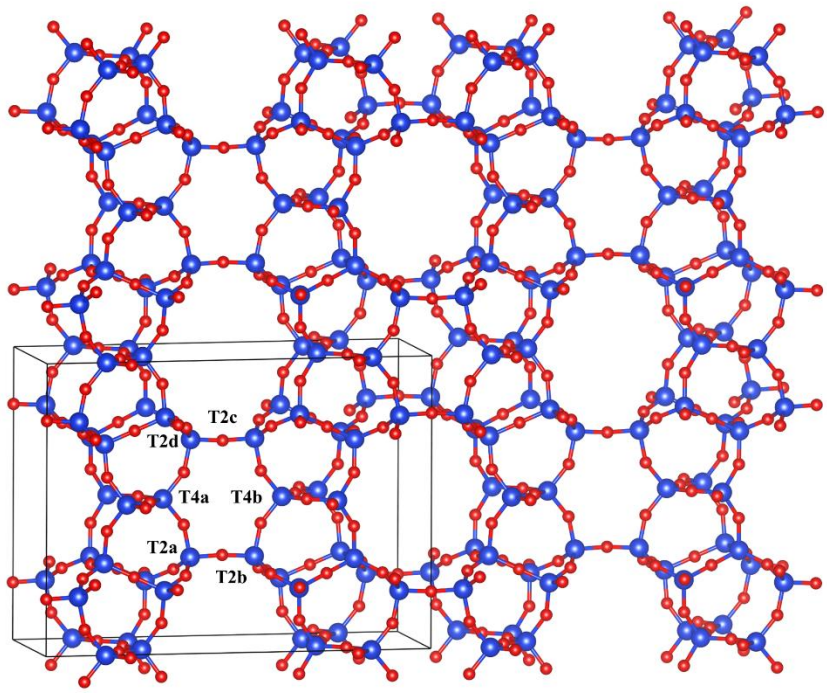


**Fig. 5 FER unit cell and its Si site with T-numbering**

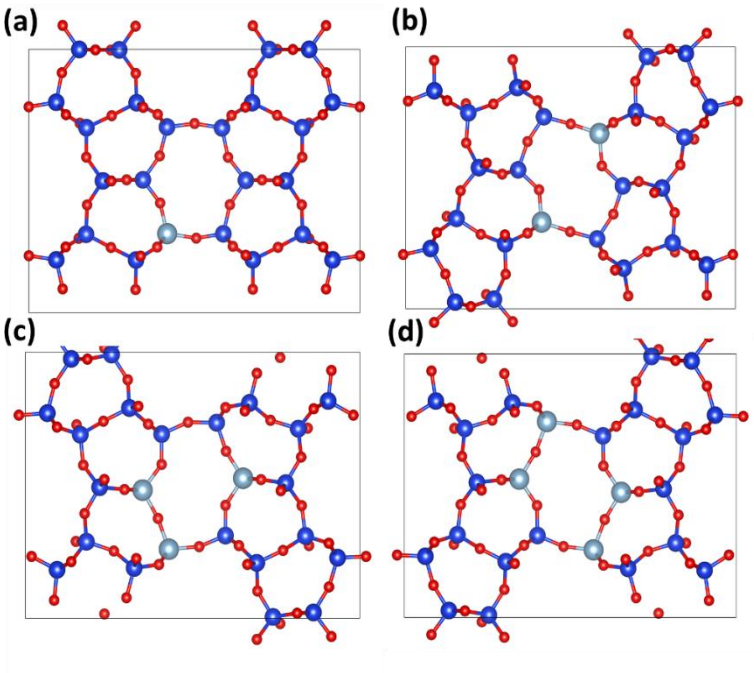


**Fig. 6 Most stable Al site 6MR of H-FERs**

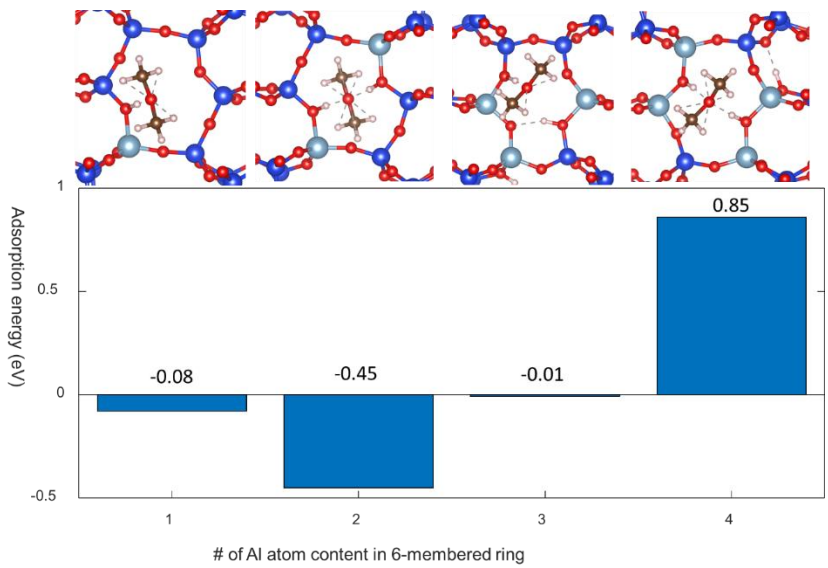


**Fig. 7. most stable dimethyl ether adsorption configuration at 6MR of H-FERs**

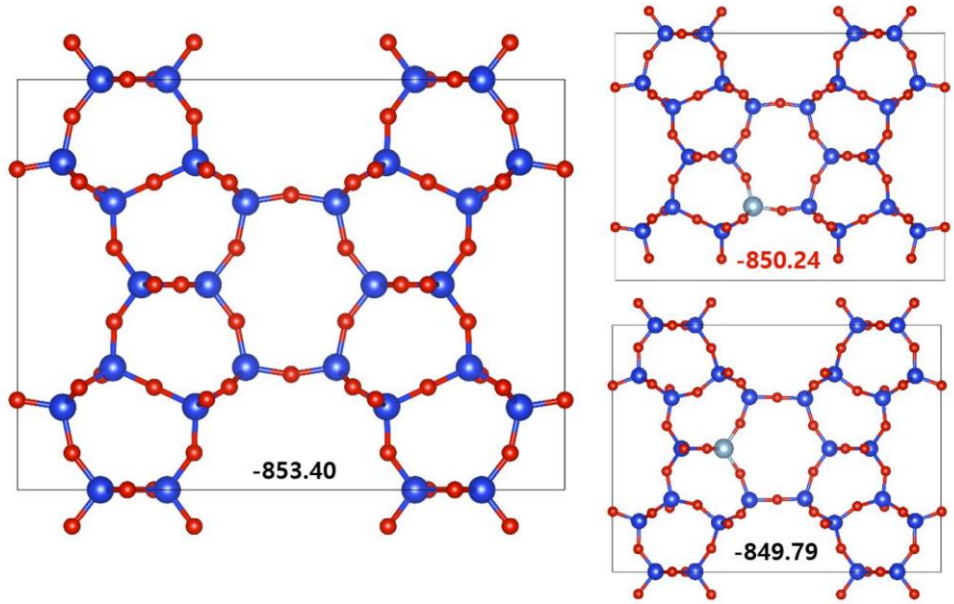


**Fig. 8 Al Configuration and energy of 6MR when one Al atom in 6MR**

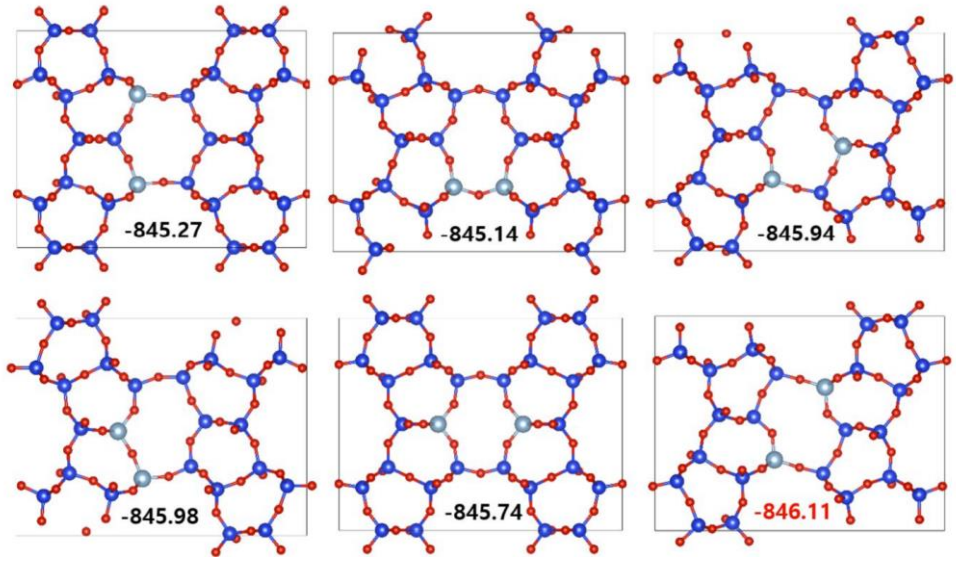


**Fig. 9 Al Configuration and energy of 6MR when two Al atoms in 6MR**

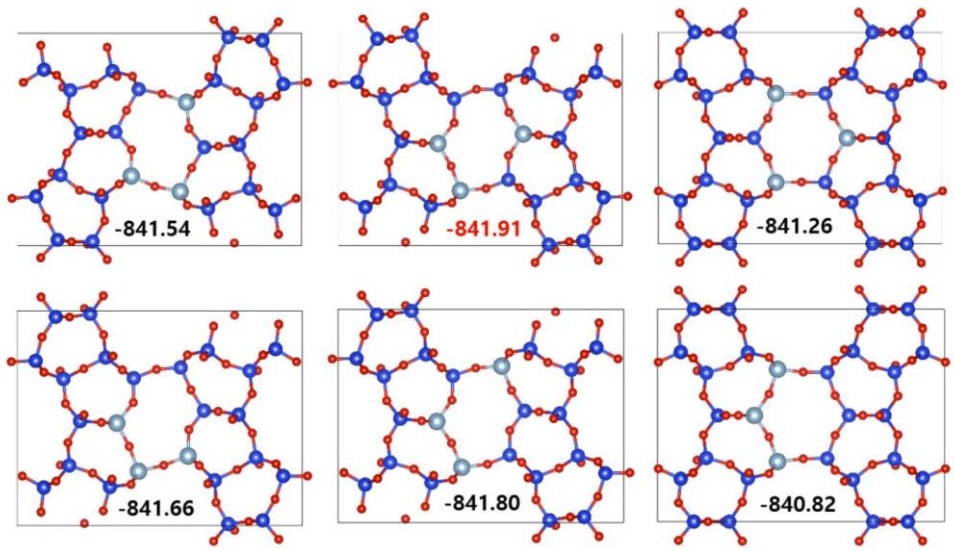


**Fig. 10 Al Configuration and energy of 6MR when three Al atoms in 6MR**

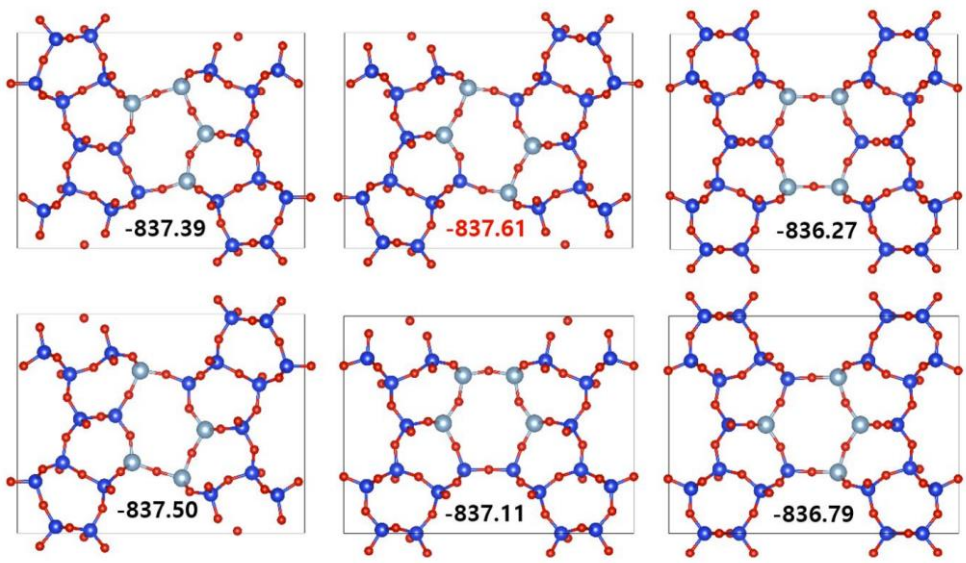


**Fig. 11 Al Configuration and energy of 6MR when four Al atoms in 6MR**

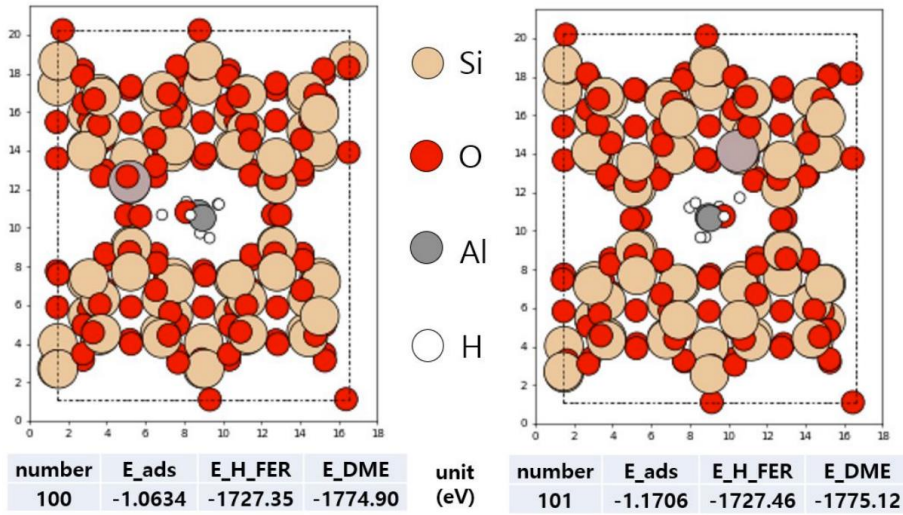


| number | E(ads) | E(H-FER) | E(DME) |
|---|---|---|---|
| 100 | -1.063 | -1727.35 | -1774.90 |
| 101 | -1.171 | -1727.46 | -1775.12 |

**Fig. 12 Energies and configurations of one Al atom in the 8-MR channels of the H-FER**

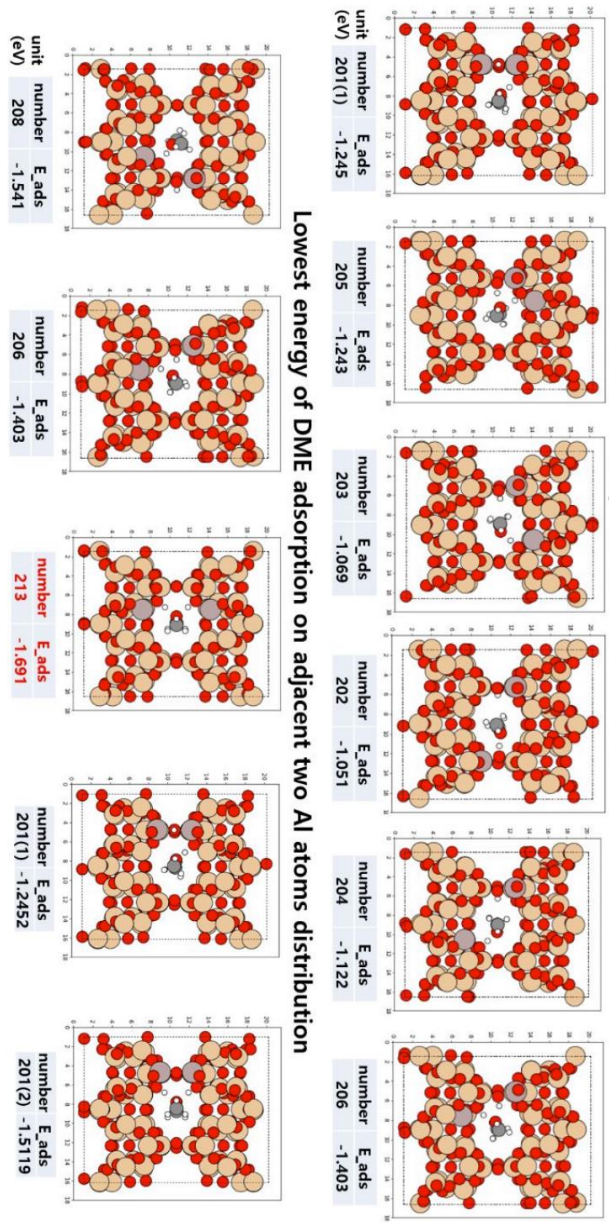


**Fig. 13 Energies and configurations of two Al atoms in the 8-MR channels of the H-FER**

| number | E(ads) | E(H-FER) | E(DME) | number | E(ads) | E(H-FER) | E(DME) |
|---|---|---|---|---|---|---|---|
| 200 | -1.090 | -1728.89 | -1776.47 | 207 | -1.244 | -1729.34 | -1777.07 |
| 201(1) | -1.245 | -1729.56 | -1777.29 | 208 | -1.541 | -1728.77 | -1776.80 |
| 201(2) | -1.512 | -1729.00 | -1777.00 | 209 | -1.123 | -1729.25 | -1776.86 |
| 202 | -1.059 | -1729.13 | -1776.68 | 210 | -0.590 | -1729.15 | -1776.22 |
| 203 | -1.070 | -1729.09 | -1776.65 | 211 | -1.015 | -1728.88 | -1776.38 |
| 204 | -1.122 | -1729.25 | -1776.86 | 212 | -1.123 | -1729.33 | -1776.94 |
| 205 | -1.243 | -1729.34 | -1777.07 | 213 | -1.691 | -1729.14 | -1777.32 |
| 206 | -1.403 | -1728.76 | -1776.65 | unit (eV) | | | |

**Table. 1 Energies of H-FER and DME adsorbed FER at each configuration of two Al atoms in the 8-MR channels.**

**(Additional explanations for DFT calculations)** Among the 13 different configurations of two Al atoms in the 8-MR channels of the H-FER, the #213 configuration was found to be most stable Al locations for DME adsorption with its lowest energy of -1.691 eV. Interestingly, the same configurations of two Al atoms (#201(1) and #201(2)) with different locations of H atoms largely altered the adsorption energy of DME molecules.

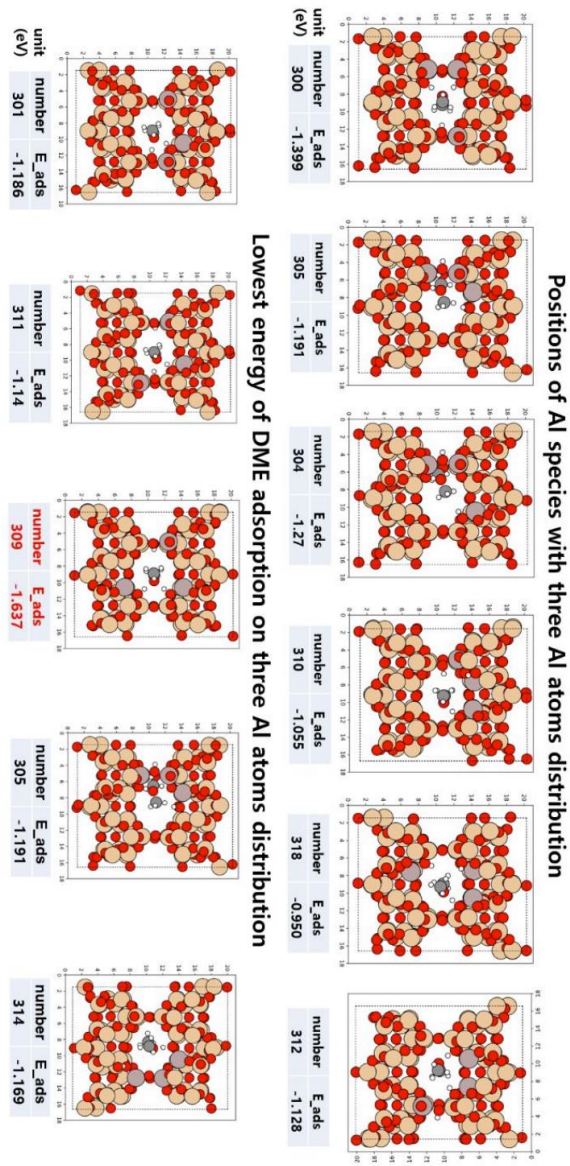


**Fig. 14 Energies and configurations of three Al atoms in the 8-MR channels of the H-FER**

| number | E(ads) | E(H-FER) | E(DME) | number | E(ads) | E(H-FER) | E(DME) |
|---|---|---|---|---|---|---|---|
| 300 | -1.399 | -1730.70 | -1778.59 | 310 | -1.055 | -1730.69 | -1778.23 |
| 301 | -1.186 | -1730.87 | -1778.54 | 311 | -1.150 | -1731.38 | -1779.02 |
| 302 | -1.307 | -1730.69 | -1778.49 | 312 | -1.128 | -1730.50 | -1778.12 |
| 303 | -1.012 | -1730.70 | -1778.20 | 313 | -0.833 | -1730.74 | -1778.07 |
| 304 | -1.270 | -1731.35 | -1779.11 | 314 | -1.169 | -1728.00 | -1775.66 |
| 305 | -1.191 | -1731.14 | -1778.82 | 315 | -1.211 | -1730.37 | -1778.07 |
| 306 | -1.397 | -1730.52 | -1778.41 | 316 | -0.975 | -1730.82 | -1778.29 |
| 307 | -0.979 | -1731.36 | -1778.83 | 317 | -1.569 | -1730.64 | -1778.70 |
| 308 | -0.948 | -1731.36 | -1778.80 | 318 | -0.950 | -1730.64 | -1778.08 |
| 309 | -1.637 | -1730.79 | -1778.91 | unit (eV) | | | |

**Table. 2 Energies of H-FER and DME adsorbed FER at each configuration of three Al atoms in the 8-MR channels**

**(Additional explanations for DFT calculations)** Among the 18 different configurations of three Al atoms in the 8-MR channels of the H-FER, the #309 configuration was found to be most stable Al locations for DME adsorption with its lowest energy of -1.637 eV. Interestingly, the same configurations of three Al atoms (#305 and #314) with different locations of H atoms largely altered the adsorption energy of DME molecules.

### 3.3.2 Comparison with experiments

Combining the calculation results so far, the following conclusions can be drawn: Al-O-(Si-O)$_2$-Al pair at 8MR in FER can enhance DME conversion, because the lowest DME adsorption energy is achieved at the Al-O-(Si-O)$_2$-Al pair configuration. To further verify the results and the effect of the Al sites in the 8-MR channels, some experimental results were compared.

The experiment was designed as follows. Three types of FER samples were synthesized, which had the same Si/Al ratio. The first sample was synthesized using piperidine as an OSDA. The second sample induced recrystallization using the first sample as a seed. Finally, recrystallization was induced in the third sample using the second sample as a seed. A detailed schematic of the synthesis is shown in Fig. 14.

As summarized in Table. 3, the relatively smaller amount of Si(1Al) sites on FER-S2 with a percentage of 19.6% in comparison to that of 24.1% on FER-S1 suggests the much greater amount of Al atoms in the 8-MR channels on FER-S2 in comparison to that of FER-S0, having an insignificant amount of Si(2Al) site. This supports that FER-S2 has the more Al-O-Si-O-Al pair in 8-MR than that in FER-S1. Since the Al-O-Si-O-Al pair is less active than the next-next nearest pair, this may cause the conversion to drop even though FER-S2 has more Al in 8-MR than FER-S1.

A deeper understanding is possible by comparing the experimental results with the DFT calculation results. In 8MR, when having Al-O-Si-O-Al pair (Al-Si-Al) and Al-O-Si-O-Si-O-Al pair (Al-Si-Si-Al), the catalyst reactivity can be considered by comparing the DME adsorption energies. In Table. 1, the configuration with Al-Si-

Al was #203, #206, and #208, and the DME adsorption energies were -1.07, -1.403, and -1.507 eV, respectively. On the other hand, the configuration with Al-Si-Si-Al was #213 and #210, and the adsorption energies were -1.691 and -1.059 eV, respectively. Therefore, the adsorption energy of DME can be minimized when it has Al-Si-Si-Al. This supports the less reactivity of FER-S2. Interestingly, in Al-Si-Si-Al, where the adsorption energy is most stabilized, two BASs act on the DME at the same time to lower the adsorption energy.

Our calculations and experimental results are consistent with the existing literature. Dedecek *et al.* showed where the most preferred Al site is according to the Si/Al content in ferrierite through DFT and $^{27}$Al MAS NMR experiments, and that the preference can change depending on the content [87]. In addition, it is revealed that the Al-O-Si-O-Al sequence is rarely distributed when Al/Si > 8, measured by $^{29}$Si MAS NMR (Table. 4) [87–89].

Thus, it is reasonably concluded that the Al Al-O-Si-O-Si-O-Al sequence mainly affect the reactivity of DME at 8MR of FER zeolite.

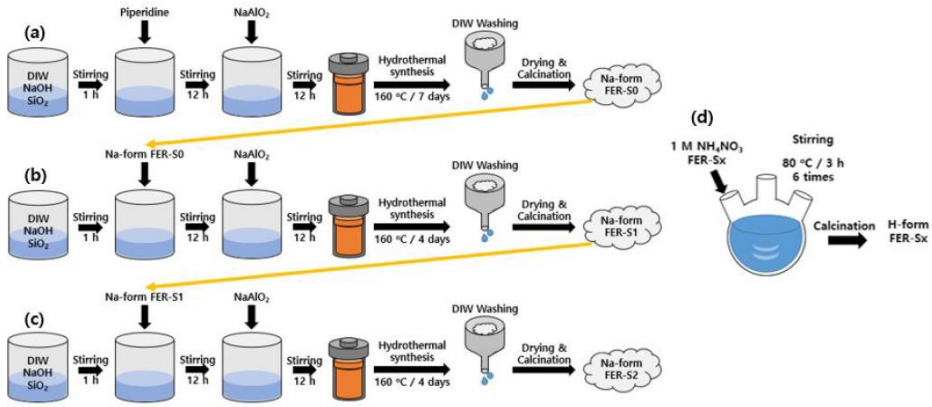


**Preparation scheme S1**. Preparation procedures of the seed-derived FERs

(**Additional explanation**) The seed-derived FERs (their quantity of ~10 g) were successively prepared by stepwise procedures as described in the preparation **Scheme S1**; (a) Synthesis of the Na-form FER-S0 through a general synthesis method, (b) Successive synthesis of Na-form FER-S1 by using the previously prepared FER-S0 seed with its content of 24 wt% and without using piperidine OSDA, (c) Successive synthesis of Na-form FER-S2 by using the prepared FER-S1 seed with its content of 24 wt% and without using piperidine OSDA, (d) Synthesis of H-form seed-derived FERs (denoted as FER-Sx) through ion-exchange method with $NH_4NO_3$ solution.

**Fig. 15 Preparation scheme of FER samples. Adapted with permission from supplementary of [57]. Copyright (2020) American Chemical Society**

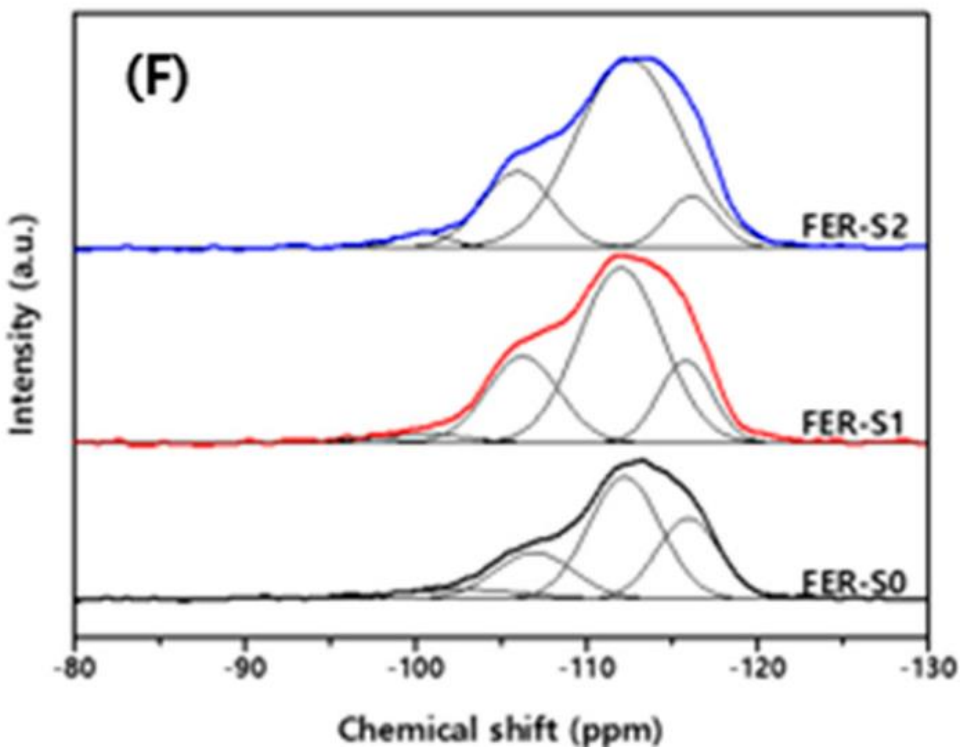


**Table. 3 Results of $^{29}$Si MAS-NMR of the seed-derived fresh FERs with the relative concentrations of the characteristic structures. Adapted with permission from supplementary of [57]. Copyright (2020) American Chemical Society**

| Catalyst | Species (%) | Si(2Al) | SiOH | Si(1Al) | Si(0Al) | Ratio of Si(2Al)/Si(1Al) |
|---|---|---|---|---|---|---|
| | Chemical shift | -99 | -101 | -105 | -111 ~ -115 | |
| FER-S0 | | - | 5.1 | 17.4 | 77.5 | - |
| FER-S1 | | 2.8 | - | 24.1 | 73.1 | 0.12 |
| FER-S2 | | 2.7 | - | 19.6 | 77.7 | 0.14 |

[a]The solid-state magic angle spinning nuclear magnetic resonance (MAS NMR) spectra of $^{29}Si$ were obtained by using a 500 MHz NMR (Varian Unity INOVA instrument) at a resonance frequency of 130.26 MHz with a 3.2 mm Chemagnetics MAS probe head at a spinning rate of 10 kHz with a reference material of $Al(NO_3)_2$ and $Si(CH_3)_4$ (TMS) as well as the delay time (D1) of 1 s at the number of scans of 4000 and $\pi/2$ pulse of 1.0 μs.

**Table. 4 Summarized results of $^{29}Si$ MAS-NMR of the seed-derived fresh FERs with the relative concentrations of the characteristic structures[a] Adapted with permission from supplementary of [57]. Copyright (2020) American Chemical Society**

## 3.4 Conclusion

In summary, all possible Al sites, and BASs in 6MR and 8MR were investigated using periodic density functional theory calculations. The most stable Al site and BAS were identified as the T2 site, which was consistent with previous papers. The adsorption energy of dimethyl ether at each BAS site was also calculated to evaluate the catalytic reactivity. The adsorption energy was optimized when two Al atoms were substituted at the two T2 sites, constructing Al-Si-Si-Al pair. The probability of Al-Si-Si-Al pairs in 8MR were measured by the $^{29}$Si MAS NMR on the FER-S0, FER-S1, FER-S2 samples. By comparing the content of the Al-Si-Si-Al in the samples, the difference of the catalytic reactivity is clearly demonstrated. This work will shed a light on understanding the relationship between the Al distribution and catalytic reactivity in ferrierite zeolites.

# Chapter 4
# Reaction mechanism of DME carbonylation over Ferrierite: First-principles Study

## 4.1 Introduction

In this section First-principles calculations were performed to suggest an elementary reaction mechanism of DME to methyl acetate (MA). Main consensus from previous section is that the Aluminum in 8-membered ring (8MR) is an active site. In the Ferrierite zeolite, there are two symmetrical Si site in 8MR, which are T2 and T4, respectively. Both Al T2 and T4 site were calculated, then it was concluded that T2 site is more stable that T4 site location. Thus, it was premised that all reaction paths break out in T2 of 8MR in FER.

Based on this, whole reaction paths on DME to MA at the 2T site of 8MR were calculated. The rate determining step (RDS) was identified and compared with that of previous reports.

## 4.2 Literature reviews

Mordenite zeolite is the first and the most focused as the catalyst for DME carbonylation. Cheng *et al.* firstly report the high selectivity of DME to MA over mordenite zeolite [52]. They argued that almost all brønsted acid sites (BAS) are

replaced by *$CH_3$ through pulse studies in HMOR and HZSM-5 catalysts. In their experiments, DME and water were detected when DME was flowed for 120 seconds by adjusting the amount and ratio of Al present in the zeolite and then Helium gas was flowed for 2 hours. Through the reaction below, it was seen that DME gas is converted into two methyl groups and water. Ratio of dosed and adsorbed DME per Al atom on zeolite is 1:1 and 0.45:1, respectively.

According to the ratio results, regardless of the amount of DME spilled (even after He post-treatment), the amount of adsorbed DME is about half of the number of Al in the zeolite, and it is suggested that H* reacts with DME and is replaced with *$CH_3$. Subsequent papers from the same group in the following year had additional results [77]. In their DME to MA reaction experiment, as in the previous paper, the DME of the same mole number as the amount of aluminum in the zeolite was pulsed shortly (pretreatment), and the DME to MA reaction was carried out in the same HMOR without any treatment with the sample washed by flowing He for 2 hours. When each proceeded, in the former case, the steady state was almost immediately reached without an induction period. In the paper, it was explained that the reason for the result was attributed to the DME, which had been flown in a pulse beforehand, had formed a methyl group on the catalyst surface in advance, and the reaction proceeded immediately, so that it reached a steady state at a rapid rate.

In the paper, this was also verified by additional experiments. After giving a DME pulse to the closed system and conducting an IR experiment, the peak change corresponding to the O-H and C-H bonds was observed, and after evacuation was performed to release the residual gas, the same IR experiment was conducted to

observe the peak change. For the close system, as the amount of DME spilled was increased, the peak corresponding to O-H bonding decreased sharply, and the C-H bonding peak corresponding to the methyl group was newly observed. After evacuation, the O-H binding peak was recovered, but the C-H binding peak was not significantly affected. Therefore, this experiment also shows that DME reacted to form a methyl group on the surface of the catalyst.

Taking the above discussion together, it was observed that in various catalysts such as MOR, SSZ-13, and ZSM-5, DME reacts with the Bronsted acid site and is almost all substituted with methyl groups. And the reaction of the produced methyl group and CO is referred to as the main RDS. Therefore, it is important to verify the proposed reaction mechanism to find out how well DME reacts and is adsorbed to the Brønsted acid site and is substituted with $CH_3$* even in the FER catalyst. If the decomposition reaction of DME to methyl group is favored in FER, the proposed mechanism is suitable. On the contrary, in FER, the reaction between the methyl group and CO on the surface is relatively dominant, and it can be argued that the DME to MA reaction may occur with another mechanism.

## 4.3 Calculation details

All density functional theory (DFT) calculations were performed by the projector augmented wave (PAW) formalism, as implemented in the Vienna Ab–initio Simulation Package (VASP) [81,82] The exchange–correlation functional, given by the generalized gradient approximation (GGA) suggested by Perdew, Burke, and Ernzerhof (PBE) [83] was used. The ferrierite unit cell containing 216 atoms ($Si_{72}$-

$_xAl_xO_{144}$) was imported from the Materials Project [21]. The structure of FER is depicted in Fig. 11. The T2 and T4 sites each are symmetrically equal at pure FER, but the symmetry is broken when Al atoms were introduced. Therefore, naming four T2 sites as a-d was introduced to distinguish each of the site.

All structures were fully relaxed to a maximum force convergence criterion of 0.01 eV $Å^{-1}$. The energy convergence threshold was set to $1 \times 10^{-8}$ eV. The cutoff energy was set to 400 eV for all calculations. Dispersion correction for the van der Waal interaction was considered by adding a pairwise interaction term to the Kohn-Sham energy using the DFT-D3 approach proposed by Grimme[84] and extended by Kerber et al. [85] which is widely applied for the theoretical investigation of adsorption and reaction in Zeolite. [86]

All adsorption energies were defined by,

$$E_{ads} = E_{FER+DME} - (E_{FER} + E_{DME})$$

where $E_{FER+DME}$, $E_{DME}$, and $E_{FER}$ are the total energies for the adsorption complex, isolated dimethyl ether (DME) molecule, and isolated zeolite, respectively.

The transition states were calculated using the climbing image nudged elastic band (CI-NEB) method [67]. Initial structure and final structure were relaxed first, and the five images are generated using the interpolation. Zeolite frameworks were fixed during CI-NEB calculation to keep convergence. The activation energies were calculated by the energy difference of the transition state and the initial state. The reaction energy also calculated by the energy difference of the final state and the initial state.

## 4.4 Results and discussion

The reaction energy paths calculated by Ferrierite are depicted in Fig.13 and Table. 5. The reaction path was suggested by Cheung *et al.* a DME is adsorbed at the BAS in 8MR and then dissociated with a methyl and a MeOH. The methyl species is attacked by CO, forming acetyl species which is suggested as a main intermediate. The acetyl specie reacts with the DME and subsequently formed a methyl acetate.

### 4.4.1 Direct dimethyl ether activation

The result calculated by Ferrierite is as follows. First, the reaction in which DME was adsorbed on the zeolite BAS and decomposed into methyl group and methanol was calculated. For this reaction, two kinds of reaction pathways were suggested: Direct decomposition type (Type 1) and decomposition via other oxygen site type (Type 2). At the type 1, the reactants, $CH_3$* and $CH_3OH$*, are simultaneously adsorbed on the Bronsted acid site and neighboring oxygen site, as depicted in Fig. 14. On the contrary, $CH_3$* is firstly adsorbed on oxygen site of zeolite and followed by the $CH_3OH$* at the type 2, as depicted in Fig. 16.

When comparing the two mechanisms, the type 1 mechanism had a higher barrier than the type 2 mechanism. The activation energy of the former is 2.902 eV, and that of the latter is 1.535 eV. It may be attributed to the repulsion interaction between two adsorption sites when reaction occurs along the type 1. Meanwhile, the two adsorption sites at type 2 mechanism are far from each other enough to neglect the repulsion interaction.

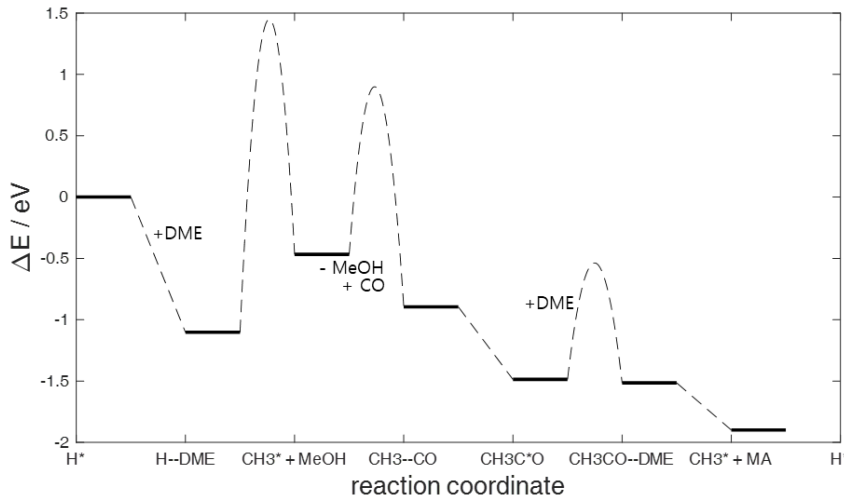


**Fig. 16 Whole reaction mechanism of DME to MA**

| REACTIONS | E (eV) | $E_{act}$ (eV) | |
|---|---|---|---|
| H* + DME → H*--DME | -1.102 | | DME adsorption |
| H*--DME → $CH_3$* + MeOH | 0.6344 | 1.54 | DME reaction |
| $CH_3$* + CO → $CH_3$--CO + * | -0.4278 | 1.36 | CO adsorption |
| $CH_3$--CO + * → $CH_3C$*O | -0.5911 | | CO reaction |
| $CH_3CO$* + DME → * + $CH_3CO$—DME | -0.0282 | 0.95 | DME adsorption |
| CH3CO--DME → $CH_3$* + MA | -0.09505 | 1.21 | Acetyl esterification |
| H* + MeOH → $CH_3$* + $H_2O$ | 0.6039 | 3.02 | methanol reaction |

**Table. 5 reaction energy and activation energy for DME to MA mechanism**

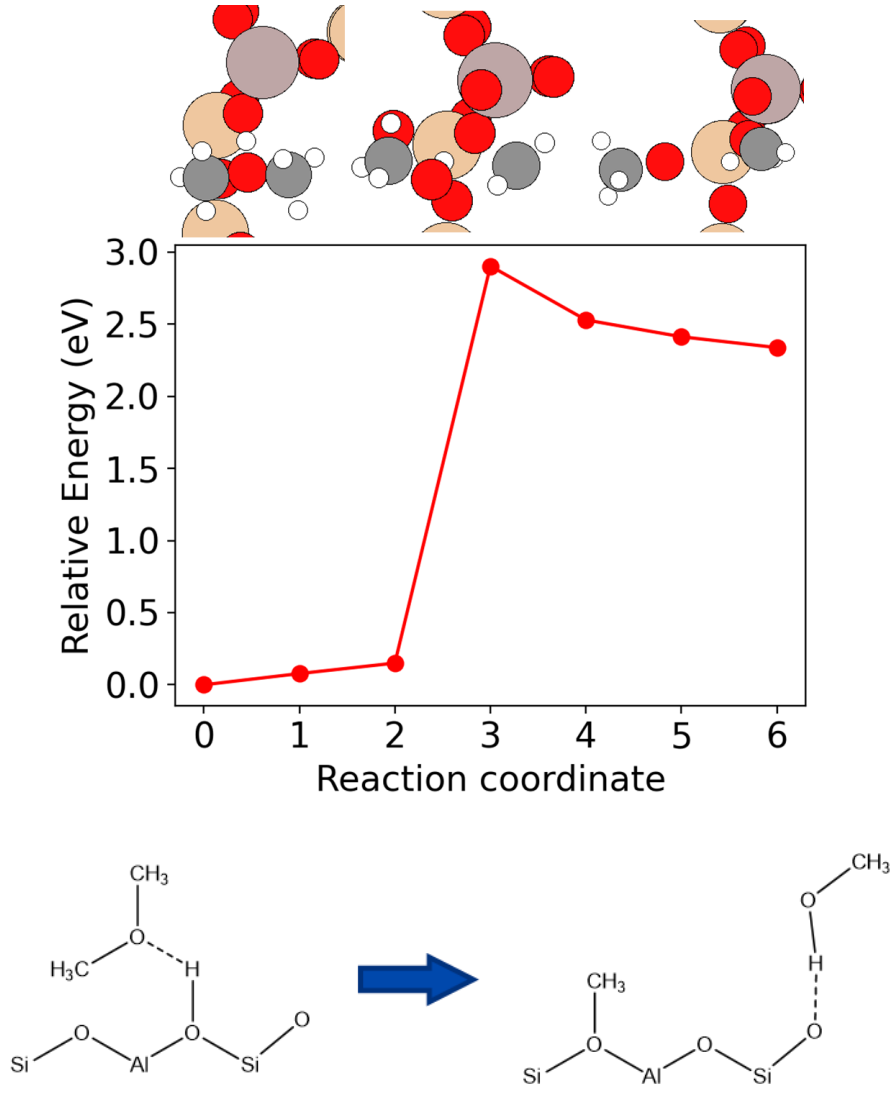


**Fig. 17 Reaction energy paths of direct decomposition mechanism.**

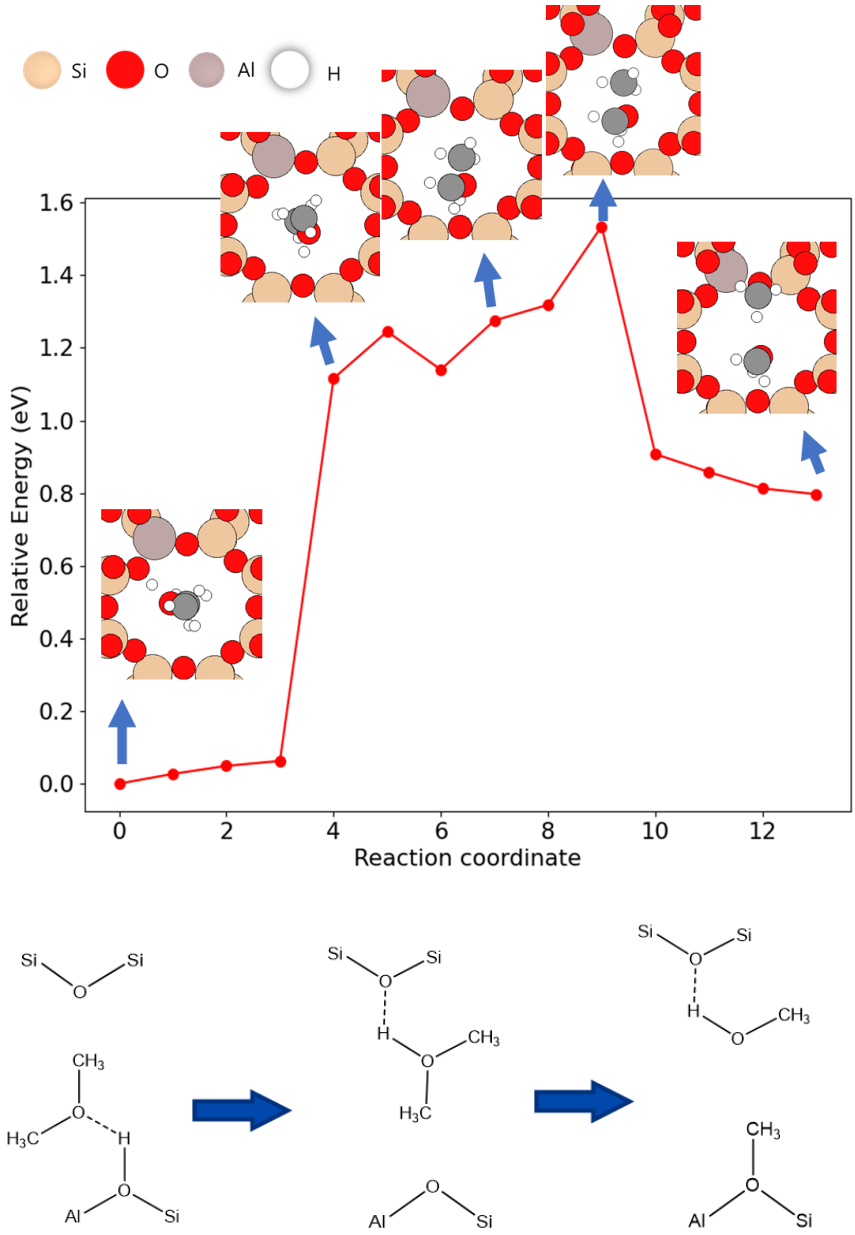


**Fig. 18 Reaction energy paths of the type 2 mechanism**

### 4.4.2 side reaction of Dimethyl ether activation

Next, it is necessary to investigate how dominant reaction of H-DME is compared to other reactions that can occur simultaneously with CO. If H-DME reacts better with DME or other intermediates other than CO, this reaction mechanism will not take place. Therefore, a series of reactions involving H-DME + DME reaction and $TMO^+$ (trimethyloxonium) were calculated by DFT, and the results are as follows.

DMEs reacted with each other to produce $TMO^+$, and the generated $TMO^+$ ions were decomposed again to generate $CH_3$* and methanol (or DME). As a result, there is no barrier to the reaction produced by $TMO^+$ and proceeds as an endothermic reaction. If the second and third reactions are summed up, it is a reaction in which DME is directly decomposed into $CH_3$* and $CH_3OH$ through the reaction of H-DME → $CH_3OH+CH_3$.

However, it can be considered that it may be a quick response because it has a lower barrier to pass through $TMO^+$ in the middle. On the other hand, the generated $TMO^+$ is very stable at 10MR, so there is little difference in $TMO^+$ form, Z-$CH_3$ state, or energy, and the barrier is also low, so it can be easily reacted to be converted into a methyl group or a methyl group can generate $TMO^+$. It has also been reported experimentally using radioactive isotopes that the reaction between DME and methyl group occurs favorable [53]. After pretreatment treatment with $^{12}CH_3O^{12}CH_3$ in HMOR, a mixed gas of $^{12}CH_3O^{12}CH_3$, $^{13}CH_3O^{13}CH_3$, and $^{12}CO$ was flowed to proceed with the DME carbonylation reaction. As a result, $^{12}CH_3O^{13}CH_3$ was produced at a high rate, and $^{12}CH_3{}^{12}COO^{13}CH_3$ was also produced. The reaction in which $TMO^+$ reacts directly with CO to produce $CH_3CO$ has a very high barrier of 4.129 eV, so the reaction seems unlikely to occur.

| State | DME+ DME-H* | $(CH_3)_3O$ + CH3OH* | DME + CH3OH + CH3*Z |
|---|---|---|---|
| Image | 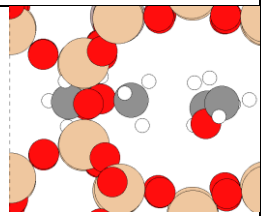 | 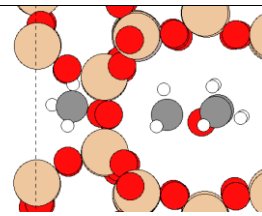 | 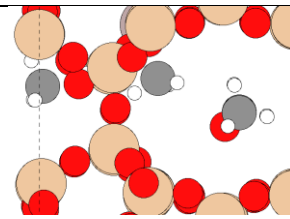 |
| E(eV) | -1820.31 | -1819.8411 | -1819.7087 |

| State | $(CH_3)_3O^+ + Z^-$ | DME+ CH3*Z |
|---|---|---|
| Image | 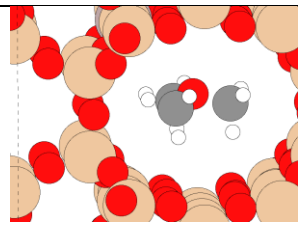 | 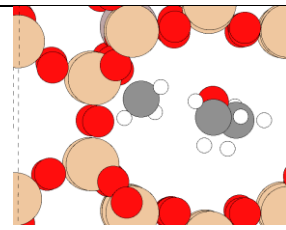 |
| Energy (eV) | -1788.9057 | -1788.9054 |

**Fig. 19 Calculated states for DME side reactions.**

| REACTIONS | ΔE (eV) | $E_{act}$ | |
|---|---|---|---|
| H* + DME → H*--DME | -1.102 | 0 | DME adsorption |
| H*--DME + DME → $(CH_3)_3O$ + $CH_3OH$* | 0.4733 | 0 | TMO generation |
| $(CH_3)_3O$ + $CH_3OH$* → DME+$CH_3OH$+$CH_3$* | 0.1324 | | TMO dissociation |
| CH3* + DME → $(CH_3)_3O$ | 0.0003 | 0.405 | TMO generation |
| CO + $(CH_3)_3O$ → $CH_3CO$ + DME | -0.9822 | 4.129 | Acetyl generation |

**Table. 6 The reaction energies and activation energy of $(CH_3)_3O$ generation paths**

### 4.4.3 C-C bond formation reaction

Both theoretical and experiments results have been reported about the surface methyl species and CO. Boronat *et al*. According to HMOR zeolite, it was argued that the selective reactivity in 8MR of DME to MA reaction is because the activation energy of DME and CO reacting with CH3* at a specific site is reversed [55]. The 10MR sites and 8MR sites of HMOR were searched, and adsorption energies for 4 substances, DME, MeOH, $H_2O$, and CO, and activation energies for methyl groups were calculated by DFT at each site. At this time, the activation energy of CO was higher than that of DME at all other sites, and it is reported that the activation energy of DME is higher than that of CO due to structural factors only at the T3-O33 site corresponding to 8MR. Therefore, it was argued that the reaction of methyl group and CO mainly occurs at this T3-O33 site, and thus MA formation also occurs selectively at this site.

In our results, the activation energy was calculated as 1.36 eV, which consistent with the previous reported data of other zeolites. However, the origin of the low activation energy is still ambiguous. To investigate it, charge density differences were calculated before and after the reaction, which are depicted in Fig. 17-18. Interestingly, the CO brings a change of charge of the inner ring space. When the CO is in the ring space, the CO molecule and oxygen atoms of zeolite structure become more negative charged. On the contrary, the surrounding space of CO becomes more positive. In addition, the space between the CO and the surface methyl species is filled with alternating positive and negative charge clouds, which mean an electrostatic interaction are applied between the two molecules.

Therefore, the charge redistribution of CO in 8MR ring cages delocalized the electron to surrounding oxygens, and the induced dipole-dipole between zeolite frameworks and CO make it possible to react feasible.

In the case of $CH_3CO^+$ specie, the charge difference was not distributed whole ring cage, but mainly occurred at the oxygens neighboring Al atoms, depicted in Fig. 18, which indicates that the induced dipole-dipole moment between zeolite framework and CO perished, and transformed to the electrostatic interaction between $CH3CO^+$ and $Z^-$.

### 4.4.4 DME – Acetyl adsorption reaction

The acetyl specie produced by C-C bond formation reaction, reacts with dimethyl ether, forming an intermediated state. The molecular configuration of the state is depicted in Fig. 19. The adsorption energy was -0.0282 eV, which is very small change. On the contrary, the activation energy of the reaction was calculated to 0.95 eV. It may be attribute to the dipole-dipole interaction between the oxygen of the DME and the carbon of the C=O in acetyl specie. The oxygen in DME has a few dipoles moment due to the C-O-C angle. The acetyl specie is a kind of cation, and the carbon of the specie has a charge deficit. Thus, these two atoms can easily attract each other to form a weak bond. The bond length of newly formed C-O was 2.32 Å, which was relatively weaker than that of C-O in DME and C=O in the acetyl specie. Bond lengths were little changed after adsorption.

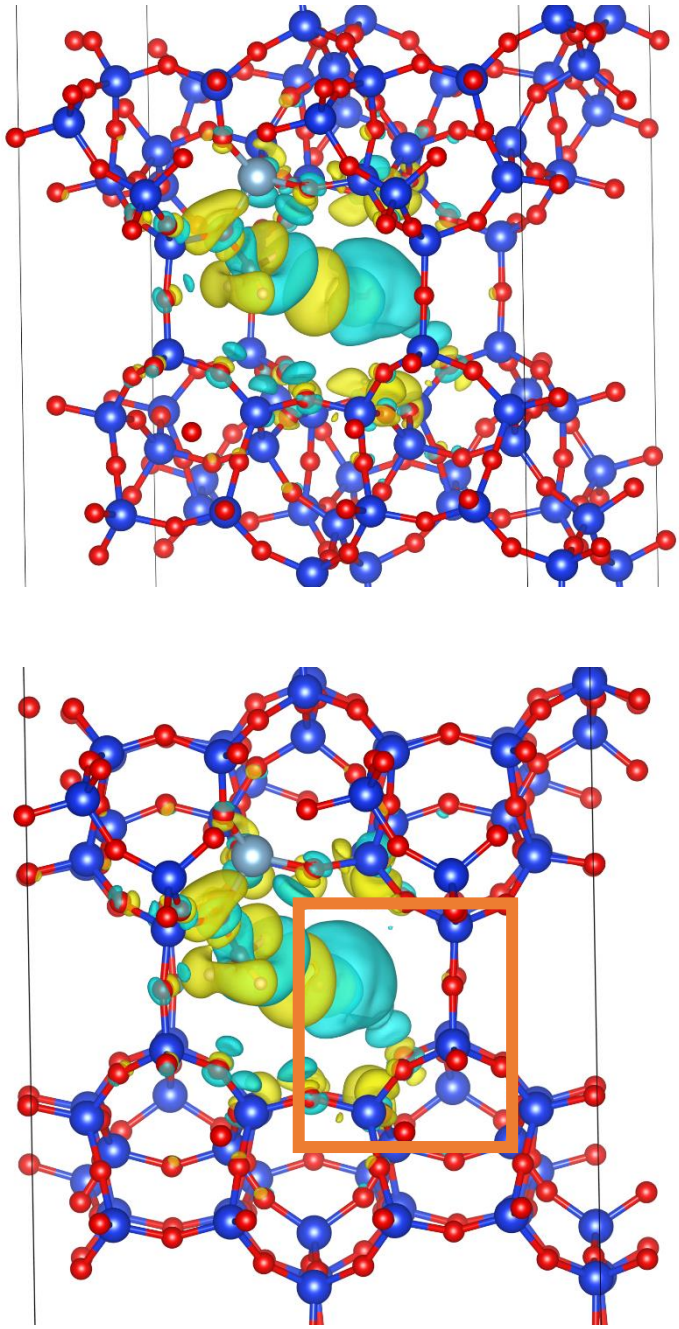

**Fig. 20 Charge density difference of CO in methyl Ferrierite. Blue region is relative electron deficit, yellow region is relative electron surplus.**

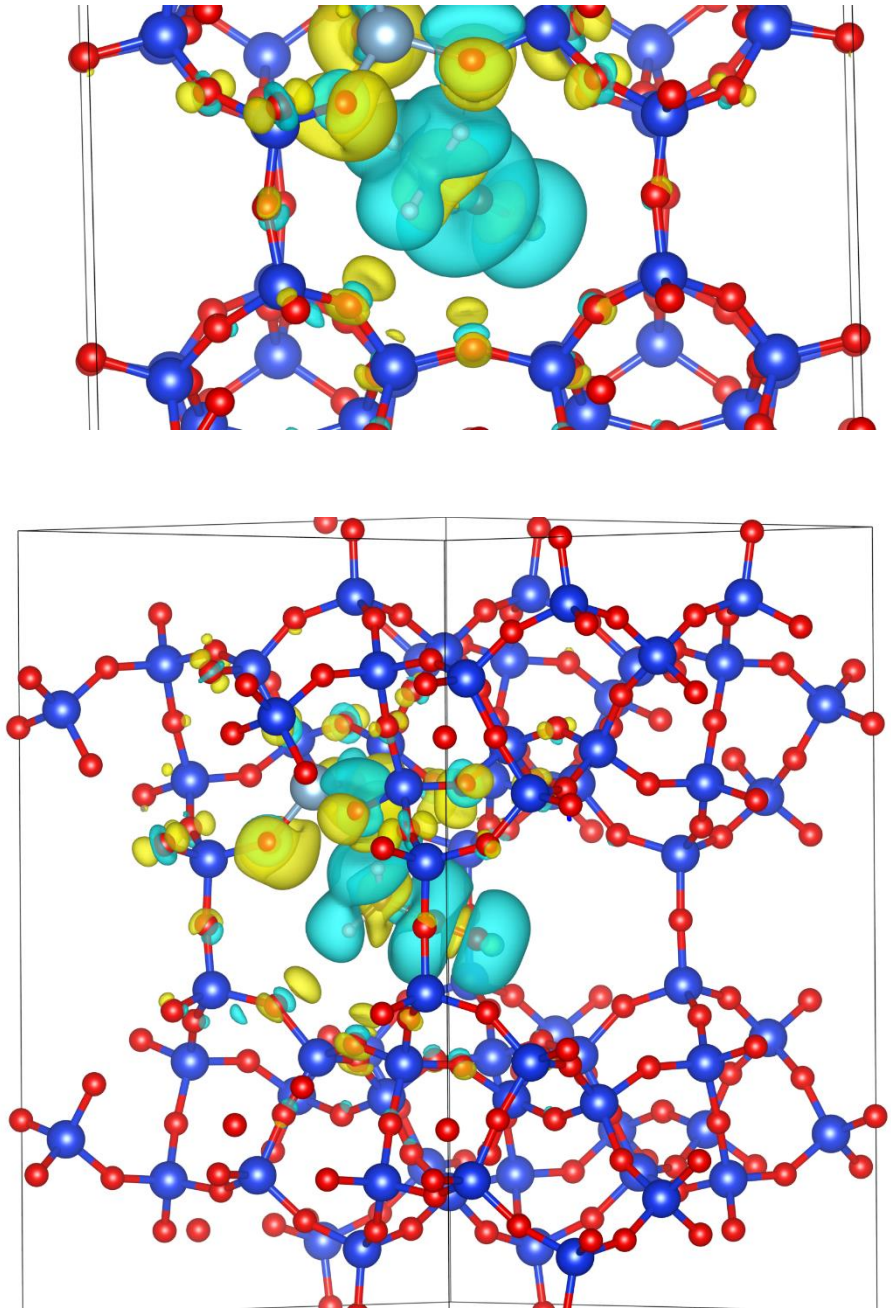

**Fig. 21 Charge density difference of $CH_3CO^+$ in Ferrierite**

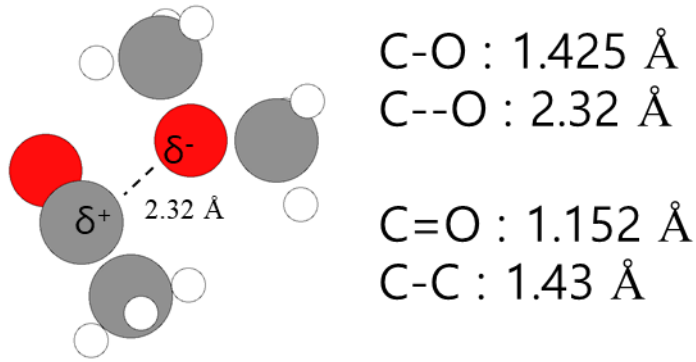


**Fig. 22. The adsorption configuration of acetyl – DME intermediate.**

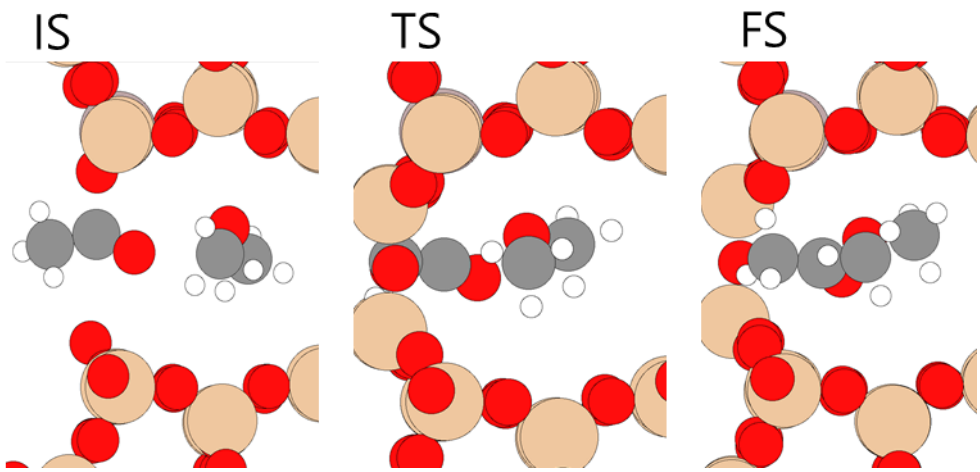


**Fig. 23 The reaction configuration of the DME and $CH_3CO$. Initial state (IS), Transition state (TS), and Final State (FS)**

### 4.4.5. Acetyl esterification

The Final stage of the reaction mechanism is the generation of MA from Acetyl esterification. The methyl ($CH_3$-) group of DME form in acetyl-DME intermediate detached to the zeolite BAS. One C-O bond breaks and one C-Oz bond creates during reaction. The reaction energy and the activation energy of the reaction is -0.095 and 1.21 eV, respectively. It is noticeable that the $CH_3$-Z is generated at the final stage of the reaction, which makes it possible to pertain the same reaction at same BAS again. It also means that the BAS is not consumed during the reaction and is retained.

## 4.5 Conclusion

In summary, firstly the most active site was searched when Al is introduced in their ring cages. As a result, T2 site at 8MR in FER is identified as a most stable site and the lowest DME adsorption site. The result was compared to experiments and confirmed a consistency. Based on the findings. The whole reaction mechanism, DME to MA were suggested and calculated using DFT calculation. To our knowledge, this is the first research about the reaction mechanism calculation for DME to MA in Ferrierite. The DME activation reaction is identified as the rate determining step and compared to previous reaction mechanism study of the other zeolite. We also tried to demonstrate the origin of the feasibility of C-C bond creation when the surface methyl species with CO. CO molecule in an 8MR ring cage induced the charge density difference and redistributed the electrons, thereby the activation energy of C-C bond formation reaction is lowered by the induced electrostatic interaction.

# Bibliography


[1] Z.J. Zhao, S. Liu, S. Zha, D. Cheng, F. Studt, G. Henkelman, J. Gong, Theory-guided design of catalytic materials using scaling relationships and reactivity descriptors, Nat. Rev. Mater. 4 (2019) 792–804. https://doi.org/10.1038/s41578-019-0152-x.

[2] A.H. Motagamwala, M.R. Ball, J.A. Dumesic, Microkinetic analysis and scaling relations for catalyst design, Annu. Rev. Chem. Biomol. Eng. 9 (2018) 413–450. https://doi.org/10.1146/annurev-chembioeng-060817-084103.

[3] M. Salciccioli, M. Stamatakis, S. Caratzoulas, D.G. Vlachos, A review of multiscale modeling of metal-catalyzed reactions: Mechanism development for complexity and emergent behavior, Chem. Eng. Sci. 66 (2011) 4319–4355. https://doi.org/10.1016/j.ces.2011.05.050.

[4] J. Greeley, Theoretical Heterogeneous Catalysis: Scaling Relationships and Computational Catalyst Design, Annu. Rev. Chem. Biomol. Eng. 7 (2016) 605–635. https://doi.org/10.1146/annurev-chembioeng-080615-034413.

[5] Z.W. Ulissi, A.J. Medford, T. Bligaard, J.K. Nørskov, To address surface reaction network complexity using scaling relations machine learning and DFT calculations, Nat. Commun. 8 (2017). https://doi.org/10.1038/ncomms14621.

[6] E.J. Mazeau, P. Satpute, K. Blöndal, C.F. Goldsmith, R.H. West, Automated Mechanism Generation Using Linear Scaling Relationships and Sensitivity Analyses Applied to Catalytic Partial Oxidation of Methane, ACS Catal. 11 (2021) 7114–7125. https://doi.org/10.1021/ACSCATAL.0C04100.

[7] N.J. Gunsalus, A. Koppaka, S.H. Park, S.M. Bischof, B.G. Hashiguchi, R.A. Periana, Homogeneous Functionalization of Methane, Chem. Rev. 117 (2017) 8521–8573. https://doi.org/10.1021/acs.chemrev.6b00739.

[8] A.A. Latimer, A.R. Kulkarni, H. Aljama, J.H. Montoya, J.S. Yoo, C. Tsai, F. Abild-Pedersen, F. Studt, J.K. Nørskov, Understanding trends in C–H bond

activation in heterogeneous catalysis, Nat. Mater. 2016 162. 16 (2016) 225–229. https://doi.org/10.1038/nmat4760.

[9] S.S.J.J. CC Wang, C–H bond activation of methane via σ–d interaction on the IrO2(110) surface: density functional theory study, J. Phys. Chem. C. 116 (2012) 6367–6370. https://doi.org/10.1021/jp300689j.

[10] S.L.M.K.M.J. G Kumar, Correlation of methane activation and oxide catalyst reducibility and its implications for oxidative coupling, ACS Catal. 6 (2016) 1812–1821. https://doi.org/10.1021/acscatal.5b02657.

[11] C.H.A.A.A.A. JF Weaver, Alkane activation on crystalline metal oxide surfaces, Chem. Soc. Rev. 43 (2014) 7536–7547. https://doi.org/10.1039/c3cs60420a.

[12] I.C. Man, H.Y. Su, F. Calle-Vallejo, H.A. Hansen, J.I. Martínez, N.G. Inoglu, J. Kitchin, T.F. Jaramillo, J.K. Nørskov, J. Rossmeisl, Universality in Oxygen Evolution Electrocatalysis on Oxide Surfaces, ChemCatChem. 3 (2011) 1159–1165. https://doi.org/10.1002/cctc.201000397.

[13] M. Rupp, A. Tkatchenko, K.-R. Müller, O.A. von Lilienfeld, Fast and Accurate Modeling of Molecular Atomization Energies with Machine Learning, Phys. Rev. Lett. 108 (2012) 058301. https://doi.org/10.1103/PhysRevLett.108.058301.

[14] F. Faber, A. Lindmaa, O.A. von Lilienfeld, R. Armiento, Crystal structure representations for machine learning models of formation energies, Int. J. Quantum Chem. 115 (2015) 1094–1101. https://doi.org/10.1002/QUA.24917.

[15] O.A. Von Lilienfeld, First principles view on chemical compound space: Gaining rigorous atomistic control of molecular properties, Int. J. Quantum Chem. 113 (2013) 1676–1689. https://doi.org/10.1002/QUA.24375.

[16] B. Meredig, A. Agrawal, S. Kirklin, J.E. Saal, J.W. Doak, A. Thompson, K. Zhang, A. Choudhary, C. Wolverton, Combinatorial screening for new materials in unconstrained composition space with machine learning, Phys. Rev. B. 89 (2014) 094104. https://doi.org/10.1103/PhysRevB.89.094104.

[17] P. Dey, J. Bible, S. Datta, S. Broderick, J. Jasinski, M. Sunkara, M. Menon, K. Rajan, Informatics-aided bandgap engineering for solar materials,

Comput. Mater. Sci. 83 (2014) 185–195. https://doi.org/10.1016/J.COMMATSCI.2013.10.016.

[18] J. Lee, A. Seko, K. Shitara, K. Nakayama, I. Tanaka, Prediction model of band gap for inorganic compounds by combination of density functional theory calculations and machine learning techniques, Phys. Rev. B. 93 (2016) 115104. https://doi.org/10.1103/PhysRevB.93.115104.

[19] F. Legrain, J. Carrete, A. van Roekeghem, S. Curtarolo, N. Mingo, How Chemical Composition Alone Can Predict Vibrational Free Energies and Entropies of Solids, Chem. Mater. 29 (2017) 6220–6227. https://doi.org/10.1021/ACS.CHEMMATER.7B00789.

[20] T. Xie, J.C. Grossman, Crystal Graph Convolutional Neural Networks for an Accurate and Interpretable Prediction of Material Properties, Phys. Rev. Lett. 120 (2018) 145301. https://doi.org/10.1103/PhysRevLett.120.145301.

[21] A. Jain, S.P. Ong, G. Hautier, W. Chen, W.D. Richards, S. Dacek, S. Cholia, D. Gunter, D. Skinner, G. Ceder, K.A. Persson, Commentary: The materials project: A materials genome approach to accelerating materials innovation, APL Mater. 1 (2013). https://doi.org/10.1063/1.4812323.

[22] C. Draxl, M. Scheffler, The NOMAD laboratory: from data sharing to artificial intelligence, J. Phys. Mater. 2 (2019) 036001. https://doi.org/10.1088/2515-7639/AB13BB.

[23] C. S, S. W, H.G.L. W, J. M, C.R. V, AFLOW: An automatic framework for high-throughput materials discovery, Comput. Mater. Sci. 58 (2012) 218. https://doi.org/10.1016/j.commatsci.2012.02.005.

[24] K.T. Winther, M.J. Hoffmann, J.R. Boes, O. Mamun, M. Bajdich, T. Bligaard, Catalysis-Hub.org, an open electronic structure database for surface reactions, Sci. Data 2019 61. 6 (2019) 1–10. https://doi.org/10.1038/s41597-019-0081-y.

[25] K. Tran, A. Palizhati, S. Back, Z.W. Ulissi, Dynamic Workflows for Routine Materials Discovery in Surface Science, J. Chem. Inf. Model. 58 (2018) 2392–2400. https://doi.org/10.1021/acs.jcim.8b00386.

[26] A.H. Larsen, J.J. Mortensen, J. Blomqvist, I.E. Castelli, R. Christensen, M. Dułak, J. Friis, M.N. Groves, B. Hammer, C. Hargus, E.D. Hermes, P.C.

Jennings, P.B. Jensen, J. Kermode, J.R. Kitchin, E.L. Kolsbjerg, J. Kubal, K. Kaasbjerg, S. Lysgaard, J.B. Maronsson, T. Maxson, T. Olsen, L. Pastewka, A. Peterson, C. Rostgaard, J. Schiøtz, O. Schütt, M. Strange, K.S. Thygesen, T. Vegge, L. Vilhelmsen, M. Walter, Z. Zeng, K.W. Jacobsen, The atomic simulation environment—a Python library for working with atoms, J. Phys. Condens. Matter. 29 (2017) 273002. https://doi.org/10.1088/1361-648X/AA680E.

[27] S. Kirklin, The Open Quantum Materials Database (OQMD): Assessing the accuracy of DFT formation energies, Npj Comput. Mater. 1 (2015). https://doi.org/10.1038/npjcompumats.2015.10.

[28] A. Jain, S.P. Ong, G. Hautier, W. Chen, W.D. Richards, S. Dacek, S. Cholia, D. Gunter, D. Skinner, G. Ceder, K.A. Persson, Commentary: The Materials Project: A materials genome approach to accelerating materials innovation, APL Mater. 1 (2013) 011002. https://doi.org/10.1063/1.4812323.

[29] Ch. Baerlocher and L.B. McCusker, Database of Zeolite Structures, (n.d.).

[30] h, Baerlocher, L.B., McCusker, Database of Zeolite structures, (n.d.). http://www.iza-structure.org/databases/.

[31] D.W. Breck, Crystalline molecular sieves, (1964).

[32] Q. Zhang, J. Yu, A. Corma, Applications of Zeolites to C1 Chemistry: Recent Advances, Challenges, and Opportunities, Adv. Mater. 32 (2020) 2002927. https://doi.org/10.1002/ADMA.202002927.

[33] J. Park, H.S. Kim, W.B. Lee, M.-J. Park, Trends and Outlook of Computational Chemistry and Microkinetic Modeling for Catalytic Synthesis of Methanol and DME, Catal. 2020, Vol. 10, Page 655. 10 (2020) 655. https://doi.org/10.3390/CATAL10060655.

[34] J. Park, J. Cho, M.J. Park, W.B. Lee, Microkinetic modeling of DME synthesis from methanol over H-zeolite catalyst: Associative vs. dissociative pathways, Catal. Today. 375 (2021) 314–323. https://doi.org/10.1016/J.CATTOD.2020.02.011.

[35] J. Park, Y. Woo, H.S. Jung, H. Yang, W.B. Lee, J.W. Bae, M.J. Park, Kinetic modeling for direct synthesis of dimethyl ether from syngas over a

hybrid Cu/ZnO/Al2O3/ferrierite catalyst, Catal. Today. (2020). https://doi.org/10.1016/J.CATTOD.2020.06.023.

[36] J.F. Haw, W. Song, D.M. Marcus, J.B. Nicholas, The mechanism of methanol to hydrocarbon catalysis, Acc. Chem. Res. 36 (2003) 317–326. https://doi.org/10.1021/ar020006o.

[37] F. Jiao, J. Li, X. Pan, J. Xiao, H. Li, H. Ma, M. Wei, Y. Pan, Z. Zhou, M. Li, S. Miao, J. Li, Y. Zhu, D. Xiao, T. He, J. Yang, F. Qi, Q. Fu, X. Bao, Selective conversion of syngas to light olefins, Science (80-. ). 351 (2016) 1065–1068. https://doi.org/10.1126/SCIENCE.AAF1835.

[38] Z. Liu, C. Sun, G. Wang, Q. Wang, G. Cai, New progress in R&D of lower olefin synthesis, Fuel Process. Technol. 62 (2000) 161–172. https://doi.org/10.1016/S0378-3820(99)00117-4.

[39] R.S. R Horn, Methane activation by heterogeneous catalysis, Catal. Lett. 145 (2014) 23–39. https://doi.org/10.1007/s10562-014-1417-z.

[40] P. Mériaudeau, V.T.T. Ha, L. Van Tiep, Methane aromatization over Mo/H-ZSM-5: on the reaction pathway, Catal. Lett. 2000 641. 64 (2000) 49–51. https://doi.org/10.1023/A:1019014431678.

[41] J. J. Spivey, Graham Hutchings, Catalytic aromatization of methane, Chem. Soc. Rev. 43 (2014) 792–803. https://doi.org/10.1039/C3CS60259A.

[42] V. Van Speybroeck, K. Hemelsoet, L. Joos, M. Waroquier, R.G. Bell, C.R.A. Catlow, Advances in theory and their application within the field of zeolite chemistry, Chem. Soc. Rev. 44 (2015) 7044–7111. https://doi.org/10.1039/c5cs00029g.

[43] M. Li, Y. Zhou, C. Ju, Y. Fang, Remarkable increasing of ZSM-5 lifetime in methanol to hydrocarbon reaction by post engineering in fluoride media, Appl. Catal. A Gen. 512 (2016) 1–8. https://doi.org/10.1016/J.APCATA.2015.12.001.

[44] U. Olsbye, S. Svelle, M. Bjrgen, P. Beato, T.V.W. Janssens, F. Joensen, S. Bordiga, K.P. Lillerud, Conversion of methanol to hydrocarbons: How zeolite cavity and pore size controls product selectivity, Angew. Chemie - Int. Ed. 51 (2012) 5810–5831. https://doi.org/10.1002/ANIE.201103657.

[45] V. Van Speybroeck, K. De Wispelaere, J. Van Der Mynsbrugge, M. Vandichel, K. Hemelsoet, M. Waroquier, First principle chemical kinetics in zeolites: The methanol-to-olefin process as a case study, Chem. Soc. Rev. 43 (2014) 7326–7357. https://doi.org/10.1039/c4cs00146j.

[46] I. Yarulina, A.D. Chowdhury, F. Meirer, B.M. Weckhuysen, J. Gascon, Recent trends and fundamental insights in the methanol-to-hydrocarbons process, Nat. Catal. (2018). https://doi.org/10.1038/s41929-018-0078-5.

[47] B.M. Weckhuysen, J. Yu, Recent advances in zeolite chemistry and catalysis, Chem. Soc. Rev. (2015). https://doi.org/10.1039/c5cs90100f.

[48] P.N. Plessow, F. Studt, Unraveling the Mechanism of the Initiation Reaction of the Methanol to Olefins Process Using ab Initio and DFT Calculations, ACS Catal. 7 (2017) 7987–7994. https://doi.org/10.1021/acscatal.7b03114.

[49] J.K. Norskov, F. Abild-Pedersen, F. Studt, T. Bligaard, Density functional theory in surface chemistry and catalysis, Proc. Natl. Acad. Sci. 108 (2011) 937–943. https://doi.org/10.1073/pnas.1006652108.

[50] C.T. Campbell, Micro- and macro-kinetics: their relationship in heterogeneous catalysis, Top. Catal. (1994). https://doi.org/10.1007/bf01492288.

[51] F. Haase, J. Sauer, Interaction of Methanol with Brønsted Acid Sites of Zeolite Catalysts: An ab Initio Study, J. Am. Chem. Soc. (1995). https://doi.org/10.1021/ja00118a014.

[52] P. Cheung, A. Bhan, G.J. Sunley, E. Iglesia, Selective carbonylation of dimethyl ether to methyl acetate catalyzed by acidic zeolites, Angew. Chemie - Int. Ed. 45 (2006) 1617–1620. https://doi.org/10.1002/anie.200503898.

[53] A. Bhan, A.D. Allian, G.J. Sunley, D.J. Law, E. Iglesia, Specificity of sites within eight-membered ring zeolite channels for carbonylation of methyls to acetyls, J. Am. Chem. Soc. 129 (2007) 4919–4924. https://doi.org/10.1021/ja070094d.

[54] A. Bhan, E. Iglesia, A link between reactivity and local structure in acid catalysis on zeolites, Acc. Chem. Res. 41 (2008) 559–567. https://doi.org/10.1021/ar700181t.

[55] M. Boronat, C. Martínez-Sánchez, D. Law, A. Corma, Enzyme-like specificity in zeolites: A unique site position in mordenite for selective carbonylation of methanol and dimethyl ether with CO, J. Am. Chem. Soc. 130 (2008) 16316–16323. https://doi.org/10.1021/ja805607m.

[56] B. Li, J. Xu, B. Han, X. Wang, G. Qi, Z. Zhang, C. Wang, F. Deng, Insight into Dimethyl Ether Carbonylation Reaction over Mordenite Zeolite from in-Situ Solid-State NMR Spectroscopy, J. Phys. Chem. C. 117 (2013) 5840–5847. https://doi.org/10.1021/JP400331M.

[57] H. Ham, H.S. Jung, H.S. Kim, J. Kim, S.J. Cho, W.B. Lee, M.J. Park, J.W. Bae, Gas-Phase Carbonylation of Dimethyl Ether on the Stable Seed-Derived Ferrierite, ACS Catal. 10 (2020). https://doi.org/10.1021/acscatal.9b05144.

[58] W. Kohn, L.J. Sham, Self-consistent equations including exchange and correlation effects, Phys. Rev. 140 (1965). https://doi.org/10.1103/PhysRev.140.A1133.

[59] M.K. Sabbe, M.F. Reyniers, K. Reuter, First-principles kinetic modeling in heterogeneous catalysis: An industrial perspective on best-practice, gaps and needs, Catal. Sci. Technol. 2 (2012) 2010–2024. https://doi.org/10.1039/c2cy20261a.

[60] H. Li, P.N. Roy, R.J. Le Roy, Analytic Morse/long-range potential energy surfaces and predicted infrared spectra for CO2 - H2, J. Chem. Phys. 132 (2010). https://doi.org/10.1063/1.3428619.

[61] P.J. Feibelman, B. Hammer, J.K. Norskov, F. Wagner, M. Scheffler, R. Stump, R. Watwe, J. Dumesic, The CO/Pt(111) Puzzle a, J. Phys. Chem. B. 105 (2001). https://doi.org/10.1021/jp002302t.

[62] G. Kresse, A. Gil, P. Sautet, Significance of single-electron energies for the description of CO on Pt(111), Phys. Rev. B - Condens. Matter Mater. Phys. 68 (2003). https://doi.org/10.1103/PhysRevB.68.073401.

[63] T.M. Soini, A. Genest, N. Rösch, Assessment of Hybrid Density Functionals for the Adsorption of Carbon Monoxide on Platinum Model Clusters, J. Phys. Chem. A. 119 (2015). https://doi.org/10.1021/acs.jpca.5b01803.

[64] A. Stroppa, K. Termentzidis, J. Paier, G. Kresse, J. Hafner, CO adsorption on metal surfaces: A hybrid functional study with plane-wave basis set, Phys. Rev. B - Condens. Matter Mater. Phys. 76 (2007). https://doi.org/10.1103/PhysRevB.76.195440.

[65] G. Rohrbach, J. Hafner, G. Kresse, Molecular adsorption on the surface of strongly correlated transition-metal oxides: A case study for CO/NiO(100), Phys. Rev. B - Condens. Matter Mater. Phys. 69 (2004). https://doi.org/10.1103/PhysRevB.69.075413.

[66] L. Schimka, J. Harl, A. Stroppa, A. Grüneis, M. Marsman, F. Mittendorfer, G. Kresse, Accurate surface and adsorption energies from many-body perturbation theory, Nat. Mater. 9 (2010). https://doi.org/10.1038/nmat2806.

[67] G. Henkelman, B.P. Uberuaga, H. Jónsson, Climbing image nudged elastic band method for finding saddle points and minimum energy paths, J. Chem. Phys. 113 (2000) 9901–9904. https://doi.org/10.1063/1.1329672.

[68] D. Sheppard, R. Terrell, G. Henkelman, Optimization methods for finding minimum energy paths, J. Chem. Phys. 128 (2008). https://doi.org/10.1063/1.2841941.

[69] J. Liu, H. Xue, X. Huang, Y. Li, W. Shen, Dimethyl Ether Carbonylation to Methyl Acetate over HZSM-35, Catal. Lett. 2010 1391. 139 (2010) 33–37. https://doi.org/10.1007/S10562-010-0411-3.

[70] J.S. Nam, A. Rong Kim, D.M. Kim, T.S. Chang, B.S. Kim, J.W. Bae, Novel heterogeneous Rh-incorporated graphitic-carbon nitride for liquid-phase carbonylation of methanol to acetic acid, Catal. Commun. 99 (2017). https://doi.org/10.1016/j.catcom.2017.06.007.

[71] A.W. Budiman, J.S. Nam, J.H. Park, R.I. Mukti, T.S. Chang, J.W. Bae, M.J. Choi, Review of Acetic Acid Synthesis from Various Feedstocks Through Different Catalytic Processes, Catal. Surv. from Asia 2016 203. 20 (2016) 173–193. https://doi.org/10.1007/S10563-016-9215-9.

[72] H. Ham, J. Kim, S.J. Cho, J.-H. Choi, D.J. Moon, J.W. Bae, Enhanced Stability of Spatially Confined Copper Nanoparticles in an Ordered Mesoporous Alumina for Dimethyl Ether Synthesis from Syngas, ACS Catal. 6 (2016) 5629–5640. https://doi.org/10.1021/ACSCATAL.6B00882.

[73] H. Ham, S.W. Baek, C.-H. Shin, J.W. Bae, Roles of Structural Promoters for Direct CO2 Hydrogenation to Dimethyl Ether over Ordered Mesoporous Bifunctional Cu/M–Al2O3 (M = Ga or Zn), ACS Catal. 9 (2018) 679–690. https://doi.org/10.1021/ACSCATAL.8B04060.

[74] S. Kattel, P. Liu, J.G. Chen, Tuning Selectivity of CO2 Hydrogenation Reactions at the Metal/Oxide Interface, J. Am. Chem. Soc. 139 (2017) 9739–9754. https://doi.org/10.1021/JACS.7B05362.

[75] G. Jia, Y. Tan, Y. Han, A Comparative Study on the Thermodynamics of Dimethyl Ether Synthesis from CO Hydrogenation and CO2 Hydrogenation, Ind. Eng. Chem. Res. 45 (2006) 1152–1159. https://doi.org/10.1021/IE050499B.

[76] K. Saravanan, H. Ham, N. Tsubaki, J.W. Bae, Recent progress for direct synthesis of dimethyl ether from syngas on the heterogeneous bifunctional hybrid catalysts, Appl. Catal. B Environ. 217 (2017) 494–522. https://doi.org/10.1016/J.APCATB.2017.05.085.

[77] P. Cheung, A. Bhan, G.J. Sunley, D.J. Law, E. Iglesia, Site requirements and elementary steps in dimethyl ether carbonylation catalyzed by acidic zeolites, J. Catal. 245 (2007) 110–123. https://doi.org/10.1016/j.jcat.2006.09.020.

[78] S. Wang, W. Guo, L. Zhu, H. Wang, K. Qiu, K. Cen, Methyl Acetate Synthesis from Dimethyl Ether Carbonylation over Mordenite Modified by Cation Exchange, J. Phys. Chem. C. 119 (2014) 524–533. https://doi.org/10.1021/JP511543X.

[79] J. Kim, H. Ham, H.S. Jung, Y. Wang, Y. He, N. Tsubaki, S.J. Cho, G.Y. Han, J.W. Bae, Dimethyl ether carbonylation to methyl acetate over highly crystalline zeolite seed-derived ferrierite, Catal. Sci. Technol. 8 (2018) 3060–3072. https://doi.org/10.1039/c8cy00329g.

[80] X. Li, X. Liu, S. Liu, S. Xie, X. Zhu, F. Chen, L. Xu, Activity enhancement of ZSM-35 in dimethyl ether carbonylation reaction through alkaline modifications, RSC Adv. 3 (2013) 16549–16557. https://doi.org/10.1039/C3RA42197J.

[81] G. Kresse, J. Furthmüller, L.D. Hicks, M.S. Dresselhaus, Effect of quantum-well structures on the thermomagnetic figure of merit, Phys. Rev. B. 47 (1993) 727–731. https://doi.org/10.1103/PhysRevB.47.12727.

[82] G. Kresse, J. Furthmüller, Efficient iterative schemes for ab initio total-energy calculations using a plane-wave basis set, 54 (1996) 11169–11186. https://doi.org/10.1103/PhysRevB.54.11169.

[83] J.P. Perdew, K. Burke, M. Ernzerhof, Generalized gradient approximation made simple, Phys. Rev. Lett. 77 (1996). https://doi.org/10.1103/PhysRevLett.77.3865.

[84] S. Grimme, Semiempirical GGA-type density functional constructed with a long-range dispersion correction, J. Comput. Chem. 27 (2006). https://doi.org/10.1002/jcc.20495.

[85] T. Kerber, M. Sierka, J. Sauer, Application of semiempirical long-range dispersion corrections to periodic systems in density functional theory, J. Comput. Chem. 29 (2008). https://doi.org/10.1002/jcc.21069.

[86] M. John, K. Alexopoulos, M.F. Reyniers, G.B. Marin, First-Principles Kinetic Study on the Effect of the Zeolite Framework on 1-Butanol Dehydration, ACS Catal. 6 (2016) 4081–4094. https://doi.org/10.1021/acscatal.6b00708.

[87] J. Dedecek, M.J. Lucero, C. Li, F. Gao, P. Klein, M. Urbanova, Z. Tvaruzkova, P. Sazama, S. Sklenak, Complex Analysis of the Aluminum Siting in the Framework of Silicon-Rich Zeolites. A Case Study on Ferrierites, J. Phys. Chem. C. 115 (2011) 11056–11064. https://doi.org/10.1021/jp200310b.

[88] J.J. Dědeček, S. Sklenak, C. Li, B. Wichterlová, V. Gábová, J. Brus, M. Sierka, J. Sauer, Effect of al-si-al and al-si-si-al pairs in the zsm-5 zeolite framework on the 27al nmr spectra. a combined high-resolution 27al nmr

and dft/mm study, J. Phys. Chem. C. 113 (2009) 1447–1458. https://doi.org/10.1021/jp8068333.

[89] J. Dědeček, L. Čapek, P. Sazama, Z. Sobalík, B. Wichterlová, Control of metal ion species in zeolites by distribution of aluminium in the framework: From structural analysis to performance under real conditions of SCR-NOx and NO, N2O decomposition, Appl. Catal. A Gen. 391 (2011) 244–253. https://doi.org/10.1016/j.apcata.2010.06.026.

[90] R.E. Fletcher, S. Ling, B. Slater, Violations of Löwenstein's rule in zeolites, Chem. Sci. 8 (2017) 7483–7491. https://doi.org/10.1039/c7sc02531a.

[91] C.J. Heard, L. Grajciar, C.M. Rice, S.M. Pugh, P. Nachtigall, S.E. Ashbrook, R.E. Morris, Fast room temperature lability of aluminosilicate zeolites, Nat. Commun. 10 (2019). https://doi.org/10.1038/s41467-019-12752-y.

[92] C.J. Heard, L. Grajciar, P. Nachtigall, The effect of water on the validity of Löwenstein's rule, Chem. Sci. 10 (2019) 5705–5711. https://doi.org/10.1039/c9sc00725c.

# 국문초록

컴퓨터 시뮬레이션 분야는 하드웨어 연산 능력의 급속한 향상에 힘입어 빠르게 성장하고 있으며, 대량 스크리닝 방법을 이용한 높은 수준의 자동화는 새로운 촉매를 설계하는 아주 핵심적인 방법론으로 주목받고 있다. 그러나 이러한 컴퓨터 시뮬레이션을 통한 새로운 촉매 발견 및 설계 연구는 촉매에 대한 인간의 이해 수준에 의해 제한된다. 특히, 이러한 자동화를 완전히 도입하기에는 아직 불균일 촉매에 대한 기본적인 이해가 부족하다. 이러한 맥락에서, 본 논문에서는 제올라이트의 디메틸에테르로부터 메틸 아세테이트까지 이르는 촉매반응에 대한 제일원리 계산을 수행하고 그 결과를 토의하여 촉매 시스템에 대한 기본적인 이해의 폭을 넓히고자 시도하였다.

논문의 내용은 4 부로 구성되어 있다. 1 장에서는 연구 동기를 제시하며, 제올라이트의 전반적인 연구 동향을 살펴보고, 디메틸에테르의 카르보닐화 반응 및 제일원리 계산을 이용한 다양한 반응모델링의 연구 배경을 살펴본다. 2 장에서는 이론적 배경을 다루었다. 밀도 함수 이론의 요약과 촉매 특성 계산 이론을 설명한다.

3 장에서는 페리어라이트 제올라이트에서 디메틸 에테르 카르보닐화 반응의 불균일 촉매 모델에 대한 원자 시뮬레이션, 특히 제올라이트에서 알루미늄 도펀트의 역할과 흡착물 분자의 제올라이트 내에서의 형상을 다루었다. 제올라이트가 일부 고리 단위의 집합체이기 때문에 구조적 복잡성과 이

구조적인 복잡성으로 인해 야기되는 흡착 에너지의 변화를 다루었으며, 실험 결과들과 함께 이 내용의 타당성을 토의하였다.

4 장에서는 제올라이트 내의 촉매 활성점에서 디메틸 에테르 카르보닐화 반응 메커니즘을 제안하고 결과 검증에 대해 논의하였다. 전체 반응 에너지를 계산하고 속도 결정 단계를 확인했고 타당성을 토의하였다. 주요 반응 경로뿐만 아니라 일부 부반응 경로도 고려했고, 그 결과를 문헌과 비교하고 논의하였다.

본 논문은 제올라이트의 촉매 반응에 대해서 원자수준에서 상세히 그 반응을 살펴봄으로써 가장 근본적인 수준에서 반응에 대한 이해도뿐만 아니라 기존 실험으로 확인하기 힘들었던 알루미늄 분포에 따른 촉매 활성에 영향도 함께 토의했다는 점에서 그 의의가 있다 하겠다.